

Segmentation of workpiece surfaces with tool marks based on high definition metrology



Yaxiang Yin^{a,b}, Yiping Shao^c, Kun Wang^{a,b}, Shichang Du^{a,b,*}, Lifeng Xi^{a,b}

^a State Key Lab of Mechanical System and Vibration, Shanghai Jiao Tong University, Shanghai, 200240, China

^b School of Mechanical Engineering, Shanghai Jiao Tong University, No. 800 Dongchuan Road, Shanghai, 200240, China

^c College of Mechanical Engineering, Zhejiang University of Technology, Hangzhou, China

ARTICLE INFO

Keywords:

Surface segmentation

Tool marks

High definition metrology

ABSTRACT

Tool marks on face-milled surfaces contain huge information about the manufacturing processes. Direct surface segmentation based on tool marks is in favor of surface error sources diagnoses. However, traditional surface segmentation methods are prone to over-segmentation when partition surfaces with tool marks. This paper proposes an improved segmentation approach to solve this problem. Based on surface topography measured by high definition metrology (HDM), the surface segmentation methodology mainly involves four steps: automatic subsurface selection, local thresh-holding, broken tool marks repairing and water segmentation (abbreviated as “STRW” methodology). A novel concept called “periodic degree” is proposed and used as the criteria of subsurface selection. A binary image of tool marks is created by an adaptive local threshold. Broken tool marks are identified by a distance threshold and repaired by a convex-hull based tool marks repairing algorithm. Finally, water segmentation is applied to divide the surface into different regions and each region belongs to a unique tool tooth trajectory. Three real cases from powertrain plant demonstrate the procedures of the methodology and verify the effectiveness of the proposed methodology.

1. Introduction

The analysis of surface topography has been increasingly important in the field of mechanical manufacturing in recent years. Surface textures at different scales impact surface functionality in different ways. For example, the intermedia scale of surface texture has significant impact on surface sealing performance. Periodic tool marks are the main components of surface texture produced by milling.

Face milling is a common machining technique to produce relative smooth surfaces to guarantee surface sealing. Fig. 1 shows the surface appearance of face milling schematically. In this paper, tool mark is conceptually defined as the local maximum of surface topography, and the section view of the milled surface in Fig. 1 shows this concept. The area between two adjacent tool marks is viewed as the region cut by one tool tooth in one revolution.

In automobile engine assembly, the top surfaces of cylinder blocks and bottom surfaces of cylinder heads are two key sealing surfaces produced by face milling. The topography of milled surfaces has direct relationship with its sealing performance. Based on experimental researches, Marie found that surface components at the intermedia scale

(corresponding to waviness) is critical for sealing performance [1]. Malburg first proposed a filtering method to relate profile waviness parameters with sealing function [2]. Later Shao et al. extended the filtering method to three-dimensional (3D) cases and proposed 3D waviness-based leakage parameters [3]. Liao et al. filtered the waviness subsurface from face-milled surface measured by high definition metrology (HDM) using wavelet decomposition, and found that the waviness subsurface mainly consists of tool marks [4]. The researches above strongly imply a relationship between tool marks and surface sealing performance. Since tool marks are directly determined by milling parameters, surface sealing can be improved by optimization of milling parameters.

The relationship between tool marks and milling parameters is investigated mainly in two ways. The first one is surface simulation, which means to input the milling parameters into models and simulate the surface topography. The second one is surface monitoring, which means the measured surface topography is the input of models, and milling parameters deduced from surface measurements are used for process monitoring. Surface simulation typically builds a dynamical model of milling processes and generates the surface topography by

* Corresponding author at: School of Mechanical Engineering, Shanghai Jiao Tong University, No. 800 Dongchuan Road, Shanghai 200240, China.

E-mail addresses: yaxiang@sjtu.edu.cn (Y. Yin), syp123gh@zjut.edu.cn (Y. Shao), wangkun1224@sjtu.edu.cn (K. Wang), lovbin@sjtu.edu.cn (S. Du), lfxi@sjtu.edu.cn (L. Xi).

<https://doi.org/10.1016/j.jmapro.2020.06.035>

Received 30 January 2020; Received in revised form 8 June 2020; Accepted 25 June 2020

1526-6125/ © 2020 The Society of Manufacturing Engineers. Published by Elsevier Ltd. All rights reserved.

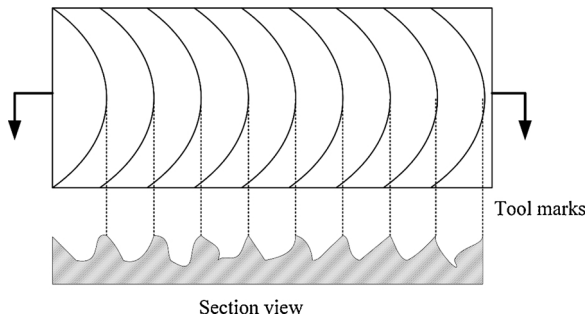


Fig. 1. Surface appearance of face milling, single tooth.

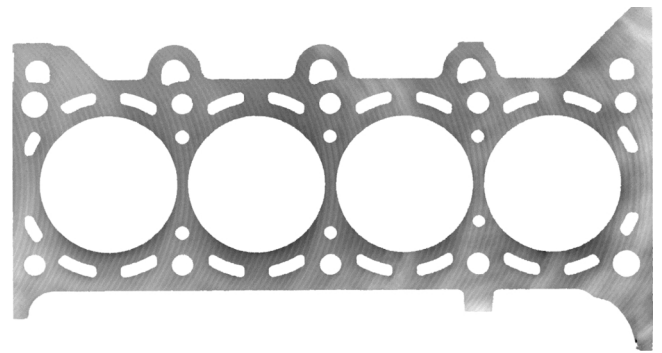


Fig. 3. The top surface from a cylinder block of automobile engines.

simulation. For example, Shun et al. proposed a numerical model integrated data from *ABAQUS* and *MATLAB* to predict surface topography produced by face milling [5]. Sun et al. presented a unified simulation model to predict 3D face-milled surface topography considering milling parameters and different kinds of initial set up errors [6]. Li et al. built a kinetic model of tool cutting to simulate the turning and milling surface topography, and studied the effect of machined surface texture on its contact performance [7].

For surface monitoring of milled surface topography, HDM is indispensable for measuring the tool marks. A recently developed HDM instrument named Shapix has been applied in automobile engine plants successfully [8]. It can measure a surface in a large view and generate a 3D height map within 40 s. The measurement resolution in *x-y*-direction and *z*-direction are 150 μm and 0.05 μm respectively. Based on this novel measurement platform, many researches have been developed, including surface quality evaluation [9], monitoring and diagnosis [3,10], surface filtering [11–14], classification [15,16] and forecasting [17,18]. A recently published book provides deeper insights into HDM based surface quality control and applications [19]. The HDM instrument and an engine block face measured by HDM are shown in Fig. 2.

With advanced HDM equipment, several milled surface monitoring methods were presented. Nguyen et al. presented modeling and experiments of a face milling process to correlate surface patterns extracted from straightened tool marks with cutting force variation [20]. Later, Nguyen et al. proposed a method to monitor the spindle setup tilt and deflection at each tool mark using HDM measured surface data [21]. Wang et al. used 3D surface form indicators extracted from tool mark images converted from HDM measurement to monitor the wear of wiper inserts [22].

A surface from a cylinder block of automobile engines is shown in

Fig. 3. The gray image is converted from point cloud of the surface measured by HDM [9]. The gray pixel values are proportional to surface heights. Moreover, periodic tool marks are observable from image vision. Tool marks contain rich information about milling processes such as tool geometry, spindle tilt and milling parameters. Currently known studies only focus on some overall statistical properties of surface variations, however, there is more information deserving to mine by studying the tool marks one by one. For instance, the tool geometry and its evolution during the machining processes can be revealed by the cross-section view (perpendicular to tool tooth trajectory) of tool marks, which is overlooked by traditional tool marks' statistics. To conduct such delicate study on each tool mark, the first step is to partition the surface topography into distinct regions. And each region belongs to a specific tool tooth trajectory and is bounded by tool marks. Therefore, a suitable surface segmentation methodology is required to fulfill the above task of partitioning.

However, there is only one published surface segmentation standard: ISO 16610–85 and it is a branch of morphological areal filters [23]. It adopts watershed segmentation using wolf pruning to partition a surface into distinct regions (hills and dales) separated by course lines and ridge lines and featured by points such as peak, pit and saddle points. However, direct application of watershed algorithm to an image is often disappointing. The image is over-segmented into a large number of small, irregular catchment basins that have no meanings. To overcome this problem, a large number of region merging algorithms were proposed [24,25]. For example, Barré and Lopez proposed to combine regions whose area is smaller than a certain threshold to its neighbors until all the segmented regions are larger than the threshold [25].

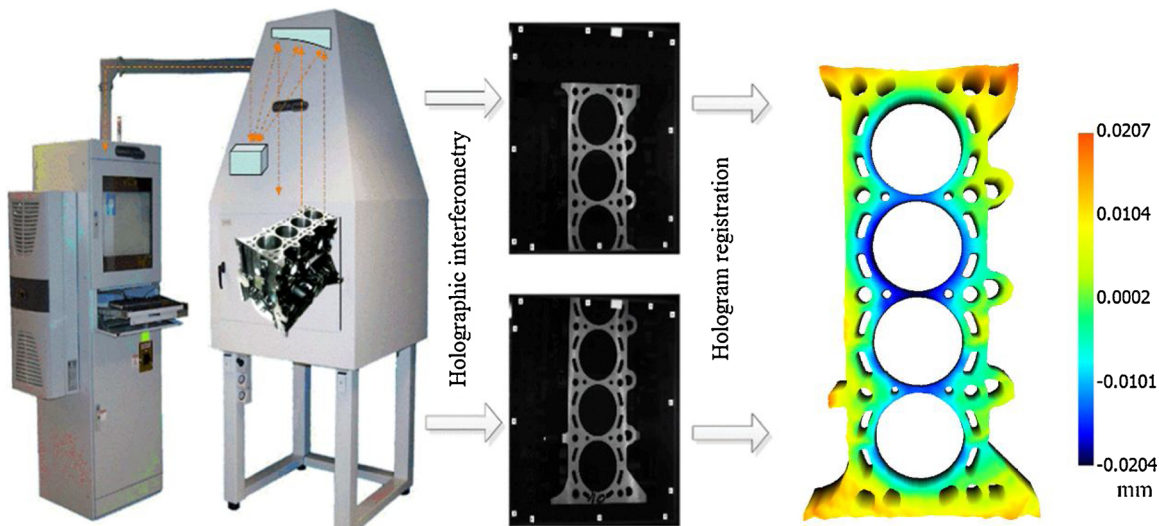


Fig. 2. Measurement by HDM.

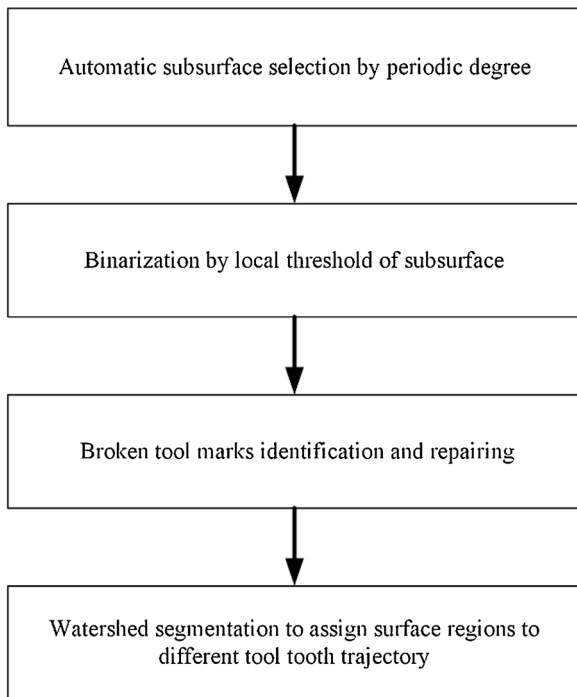


Fig. 4. Framework of the proposed STRW surface segmentation methodology.

The traditional watershed segmentation and its extensions have gained success on some kinds of machined surfaces especially surfaces with particle features. For example, a grinding wheel surface and a car body panel shown in ISO 16610–85 have a satisfactory segmentation [23]. The concepts of watershed segmentation are originally from geomorphology. It provides a new view of machined surface topography and has a close relationship with surface functionality. However, it has a major weakness: for surfaces who have no particle features

such as turning and milling surfaces, its segmentation results are often unsatisfactory and have no relation with the machining processes. The contribution of this paper is to solve this problem by proposing an improved segmentation methodology. The methodology developed in this paper could be an important complement and extension to ISO 16610–85 and it is a first trial to relate surface topography with machining processes by surface segmentation.

The surface segmentation methodology mainly consists of four steps: automatic subsurface selection by periodic degree, local thresholding to enhance tool marks, broken tool marks identification and repairing, and watershed segmentation. This methodology is named as “STRW” (subsurface selection, local thresh-holding, tool marks repairing and watershed segmentation) according to the key operation of each step.

The remainder of this paper is organized as follows. A detailed description of the proposed “STRW” methodology is presented in Section 2. In Section 3, three case studies demonstrate the effectiveness of the proposed methodology and compares the segmentation result with multiscale watershed segmentation. Section 4 discusses the limitation of “STRW” methodology and future improvement direction.

2. The proposed methodology

The overview of “STRW” segmentation methodology is shown in Fig. 4. It mainly consists of the following four steps.

Step1: Since direct measured surface only shows the tool marks pattern implicitly, for convenience of extracting tool marks in next steps, it must be filtered first to get the subsurface that shows tool marks more clearly. However, the spatial frequency of tool marks is unknown, the most suitable subsurface for tool marks extraction can only be selected manually according to engineers’ experiences. To achieve automatic subsurface selection, a novel concept “periodic degree” is proposed in this step and the subsurface with highest periodic degree is proved to be the most suitable subsurface for tool marks extraction.

Step2: To separate tool marks from its background clearly, thresholding method is applied to the selected subsurface. Subsurface may

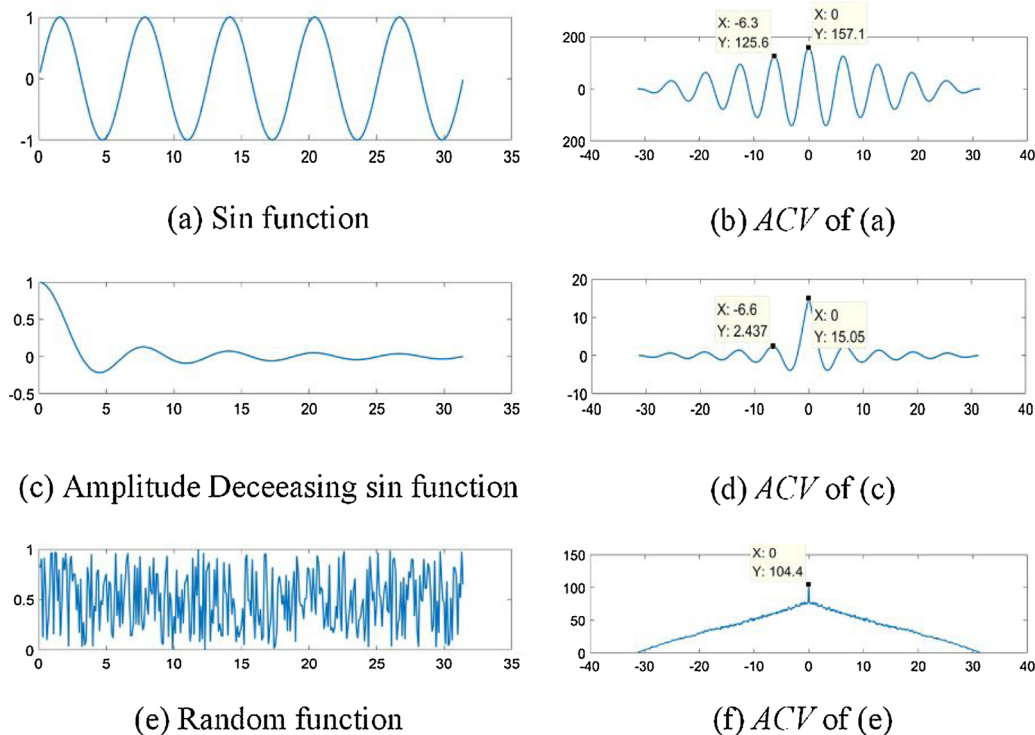


Fig. 5. Three types of function with different PD and their ACV.

have a fluctuated form error and such fluctuation has a negative effect on tool marks extraction. To overcome this negative effect, a local thresh-holding method is proposed in this step. Local threshold is determined only on the properties of a small neighborhood of a point, so it can adapt to surface fluctuations. Therefore, a binary image of tool marks is created by applying a local thresh-holding method to the selected subsurface.

Step3: After thresh-holding, the tool marks are separated from its background. However, due to irregularities of real surfaces, breakage may occur in tool marks. Tool marks with breakage are identified by an adaptive distance threshold, and they are repaired by a convex-hull based tool marks repairing algorithm.

Step4: The final step is to partition the surface into regions that belong to different tool tooth trajectories. Based on the former three steps, direct application of watershed segmentation to the binary image after tool mark repairing can result in a satisfactory segmentation.

2.1. Automatic subsurface selection by periodic degree

Direct measured surface only shows the tool marks pattern implicitly, for convenience of extracting tool marks, it must be filtered first and to find the subsurface which shows tool marks most clearly. Since tool marks have a fixed frequency, the subsurface that contains tool marks must have a dominant periodic feature. ISO 25178–2 has defined many kinds of surface texture parameters, such as texture aspect ratio (S_{tr}) and auto-correlation length (S_{al}) [26]. S_{al} is related to the wavelength of the main frequency components of surfaces, and S_{tr} is a measure of surface anisotropy. However, there is no existing parameter to measure the periodic degree of a surface.

To quantify the periodic level of a profile or surface, a novel concept called “periodic degree” (PD) is proposed in this section. Three types of function with different periodic level is shown in Fig. 5(a), (c) and (e). It is obvious that the function 5(a) has a maximum periodic level while function 5(e) has a minimum periodic level. The 1D auto-covariance function (ACV) (defined in Eq. (1)) shown in Fig. 5 (b), (d) and (f) reflects the periodicity difference clearly, so PD can be defined as a ratio of the secondary peak height (H_{sp}) to the highest peak height (H_{hp}), as shown in Eq. (2). And the corresponding periodic degrees are $PD_a = 125.6/157.1 = 0.80$, $PD_c = 2.44/15.05 = 0.16$, $PD_e = 0$, consistent with vision observation. It is worth noting that the definition of “peak” in this paper is a local maximum with an uphill path and a downhill path with respective least path length of three. According to this definition, Fig. 5(f) has no peaks, and in this situation, the periodic degree is set to be zero.

$$ACV(i') = \frac{1}{nx} \sum_{i=1}^{nx-i'} y(i)y(i+i'), 0 \leq i' \leq nx-1 \tag{1}$$

$$PD = \frac{H_{sp}}{H_{hp}} \tag{2}$$

$$y_i \in Peak \text{ if } \begin{cases} y_i > y_{i-1} > y_{i-2} > y_{i-3} \\ y_i > y_{i+1} > y_{i+2} > y_{i+3} \end{cases} \tag{3}$$

The definition of auto-covariance function, corresponding “peak” and periodic degree can be extended to 2D cases. The areal auto-covariance function ($AACV$) for 3D surfaces is defined by Eq. (4).

$$AACV(j', i') = \frac{1}{nx \cdot ny} \sum_{i=1}^{nx-i'} \sum_{j=1}^{ny-j'} z(j, i)z(j+j', i+i'), 0 \leq j' \leq ny-1, 0 \leq i' \leq nx-1 \tag{4}$$

The 2D periodicity degree is defined the same as 1D cases, namely,

defined as Eq. (2). The “peak” is defined as any point that rises above forty-eight nearest neighbors, as shown in Fig. 6. The distance between two points in 2D cases are defined as the chessboard distance, as shown in Eq. (5). Therefore, the distance of yellow points, orange points and green points to P are 1, 2 and 3 respectively. So in 2D cases, a peak is formally defined as Eq. (6), consistent with its 1D definition.

$$d(P_{mn}, P_{ij}) = \max(|m-i|, |n-j|) \tag{5}$$

$$z_{ij} \in Peak \text{ if } z_{ij} > z_{mn} > z_{pq} > z_{st}, d(z_{ij}, z_{mn}) = 1, d(z_{ij}, z_{pq}) = 2, d(z_{ij}, z_{st}) = 3 \tag{6}$$

By calculating the periodic degree of the auto-covariance function of different subsurfaces, the subsurface with maximum periodic degree is selected as the most suitable subsurface for tool marks extraction.

To demonstrate this subsurface selection algorithm, a simulated surface (Eq. (7)) is tested,

$$z(x, y) = -0.5 \cos(2\pi x/6.4) + 0.1 \cos(2\pi x/3) + 0.05x + 0.05y + 0.05randn(256) \tag{7}$$

where cosine term of wavelength 6.4 is regarded as periodic tool marks, cosine term of wavelength 3 is the simulated periodic noises, and the last three terms are regarded as form error and random noises.

The area of simulated surface is 51.2 mm × 51.2 mm and sample spacing is 0.2 mm in horizontal directions. A biorthogonal wavelet (bior4.4) decomposition is applied to this surface and it is decomposed into five levels. Fig. 7(a) shows the simulated surface in 3D form. Fig. 7(b) ~ (f) are images of decomposed subsurface $D_1 \sim D_5$ (define $D_i = D_i^H + D_i^V + D_i^D$, and wavelet decomposition is a recursive form of $A_i = A_{i+1} + D_{i+1}$). From vision observation, Fig. 7(e) seems to have a strongest periodic degree. The AACV of subsurfaces are plotted in Fig. 8, and the last three graphs are similar and the most periodic subsurface cannot be determined from vision. The periodic degree defined in this section are calculated and listed in Table 1, and D_4 has the largest value, which is consistent with observation from Fig. 7. So in this step, subsurface D_4 is selected.

2.2. Binarization by local thresh-hold of subsurface

To separate tool marks from its background, an image thresh-holding method is applied, and the thresh-holding method is defined as Eq. (8).

$$B(x, y) = \begin{cases} 1 \text{ if } I(x, y) > T \\ 0 \text{ if } I(x, y) \leq T \end{cases} \tag{8}$$

There are two common thresh-holding methods: global thresh-holding and local thresh-holding. Classical global thresh-hold method is the Ostu’s method [27]. An optimal threshold T^* is found to achieve maximum inter-class variance. An improved adaptive approach is to compute a threshold at every point (x, y) in the image based on specified properties computed in a neighborhood of (x, y) . In this algorithm, the standard deviation and mean of the heights in the neighborhood of a point are used to determine the local threshold. Let σ_{xy} and m_{xy} denote the standard deviation and mean value of the heights of adjacent points centered at (x, y) . The local threshold is defined as Eq. (9), where a and b are nonnegative constants.

$$T_{xy} = a\sigma_{xy} + bm_{xy} \tag{9}$$

To illustrate the adaptability of local thresh-holding method, the surface simulated by $z(x, y) = -0.5 \cos(\frac{2\pi x}{6.4}) + 0.05x + 0.05y$ is taken for an example. Fig. 9(a) shows the image form of this surface and it has clear periodic marks with a gradient background. Fig. 9(b) shows the image after global thresh-holding using Ostu’s method and it doesn’t capture the periodic marks. Fig. 9(c) shows the image after local thresh-holding (the neighborhood region is a window size of 7×7 , and

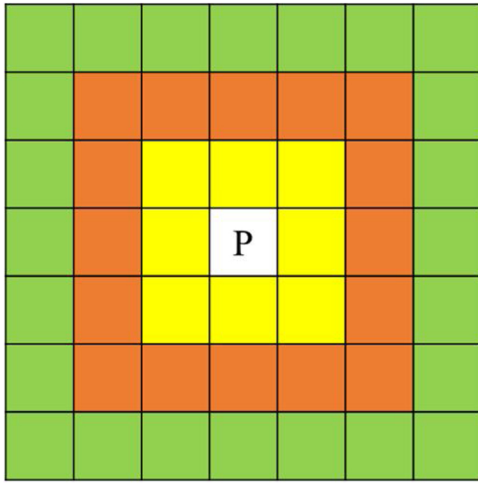


Fig. 6. A 2D peak and its neighbors.

$a = 1.5, b = 1$), it captures the periodic marks successfully.

2.3. Broken tool marks identification and repairing

After local thresh-holding, the tool marks may not be perfect as expected because of some machining errors. A common situation is the unexpected breakage of continuous tool marks as shown in Fig. 10(a). Unexpected breakage of continuous tool marks will bring obstacles to correct segmentation. Naturally, it is desired to develop an algorithm to automatically repair the breakage as Fig. 10(b) shows.

To repair the breakage of tool marks, the broken parts of marks must be identified firstly. Since the size of breakage gap of tool marks is usually smaller than the distance of adjacent tool marks. The inter-region distance (IRD) matrix can be utilized to distinguish broken marks

from adjacent marks. The elements $IRD(i,j)$ represents the minimum distance between region labeled i and another region labeled j and it is defined by Eq. (10).

$$IRD(i, j) = \min \sqrt{(x_p^i - x_q^j)^2 + (y_p^i - y_q^j)^2} \quad (p = 1, 2, \dots, N_i, q = 1, 2, \dots, N_j, i \neq j) \quad (10)$$

where N_i is the number of points in region X_i and N_j is the number of points in another region X_j . And $\min(IRD)$ is a vector containing the minimum value of each column from the matrix IRD . The maximum of $\min(IRD)$ is approximately the distance between adjacent tool marks. So the adaptive distance threshold DT to distinguish broken marks from adjacent marks can be set to be a proportion of $\max(\min(IRD))$ according to engineering experiences (a proportion coefficient C between 0.5 and 0.9 is recommended), and DT is defined by Eq. (11).

$$DT = C \times \max(\min(IRD)) \quad (11)$$

If $\min(IRD(i))$ is less than DT , then the region labeled i can be assigned to the group of broken tool marks. Otherwise, the region labeled i should be assigned to the group of continuous tool marks. By repairing the group of broken tool marks and adding the group of continuous tool marks, the image of fully repaired tool marks could be obtained. This thought of dividing and repairing is summarized in Fig. 11.

The “tool mark repairing” algorithm is designed to deal with the sub image containing all broken tool marks. A “convex hull” generation algorithm is adopted to help the tool marks repairing.

In mathematics, the convex hull of a points set S in the Euclidean plane is the smallest convex set that contains S and it is also the set of all convex combinations of points in set S . The formal definition of convex hull could be expressed as formula (12),

$$Conv hull(X) = \left\{ \sum_{i=1}^{|X|} \alpha_i x_i \mid \forall i: \alpha_i \geq 0 \wedge \sum_{i=1}^{|X|} \alpha_i = 1, x_i \in X \right\} \quad (12)$$

where $|X|$ denotes the number of points in set X . Fig. 12(a) shows an

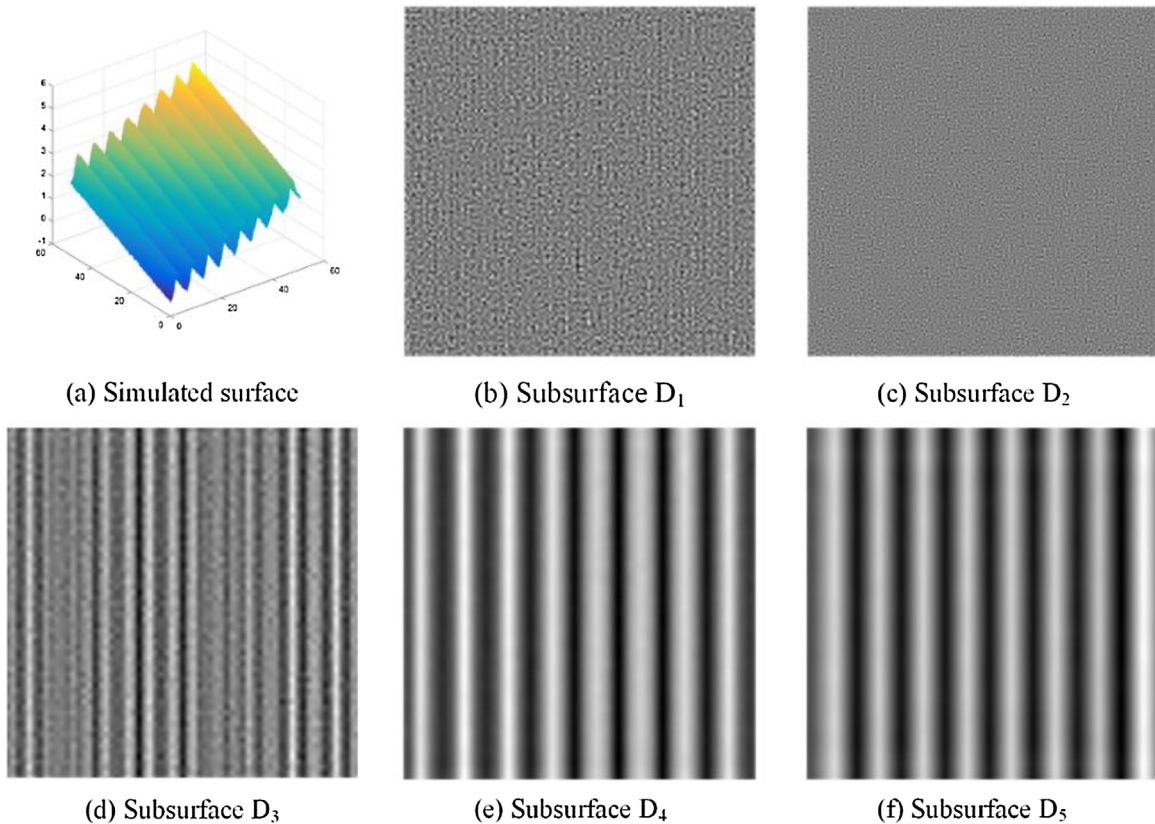


Fig. 7. Simulated surface and decomposed subsurfaces.

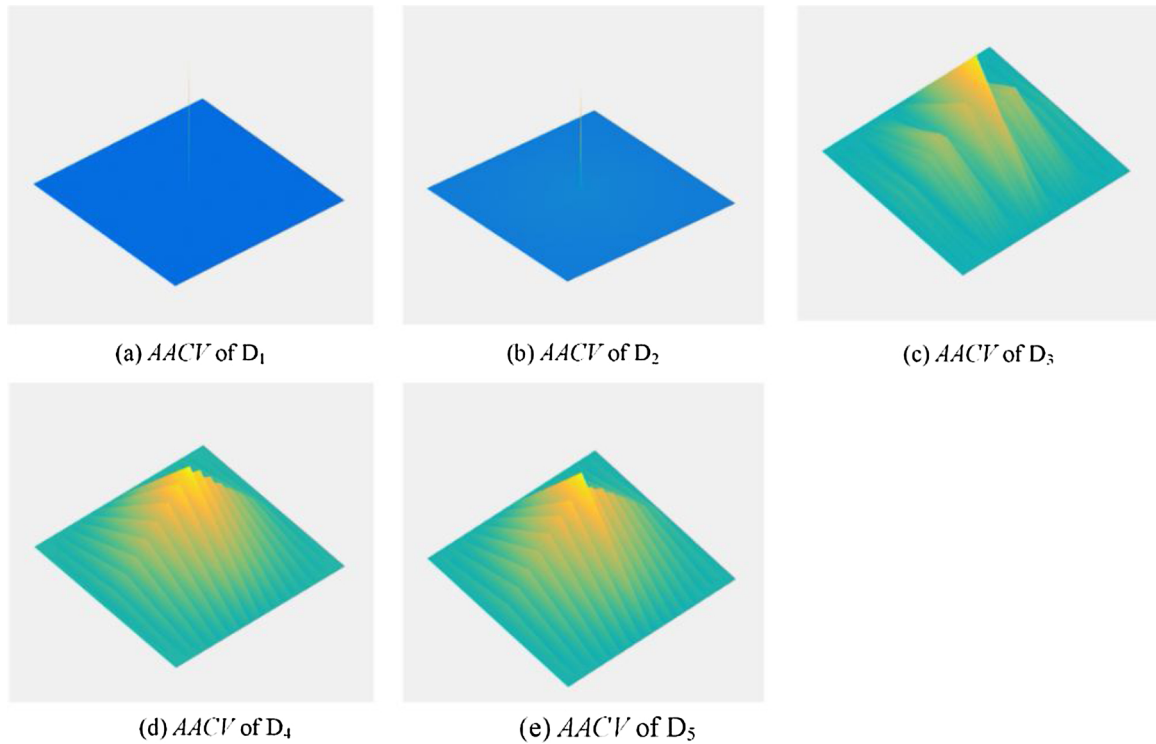


Fig. 8. AACV plots of subsurfaces.

example of a set of points and its convex hull. The idea of repairing the breakage by convex hull is illustrated in Fig. 12(b). First, find the edge points near the breakage gap, then construct a convex hull of the points set, finally fill the convex hull region. The quickhull algorithm for convex hull [28] is adopted to generate the convex hull connecting the broken parts. The detailed procedures of tool mark repairing algorithm are demonstrated in Fig. 13.

To illustrate the repairing ability of the proposed algorithm, a simple example of broken marks is taken for demonstration. Fig. 14(a)

shows the simulated tool marks with breakage, and the sub image *BW_broken* and sub image *BW_connected* are shown in Fig. 14(b) and (c) respectively. The convex hulls used to repair the breakage are plotted with red boxes in Fig. 14(d). The sub image of repaired tool marks *BW_repaired* and corresponding full image *BW_full* are shown in Fig. 14(e) and (f) respectively.

Table 1
Periodic degree of decomposed subsurface $D_1 \sim D_5$.

Subsurface	D_1	D_2	D_3	D_4	D_5
Periodic degree	0.013	0.086	0.539	0.742	0.693

2.4. Watershed segmentation

After repairing broken tool marks, the periodic tool marks pattern has been clearly shown. However, for surface segmentation, dividing line of one-pixel width is desired to achieve better segmentation accuracy. The task of this final step is to thin tool marks to one-pixel width, and keep the thinned tool marks as close to the centerline of the origin tool marks as possible.

Fortunately, classical water segmentation could help to fulfill this task. Fig. 15(a) shows a simulated diagonal tool mark, and the dividing

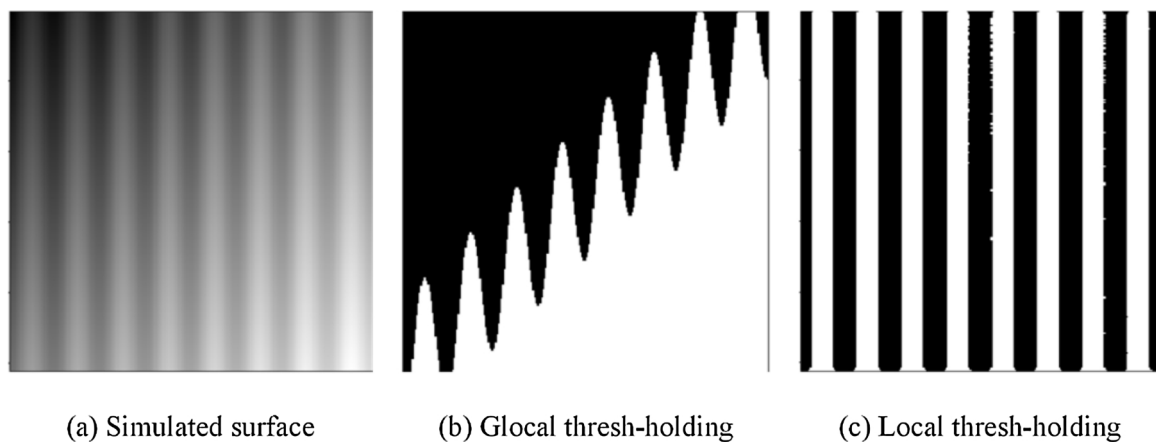
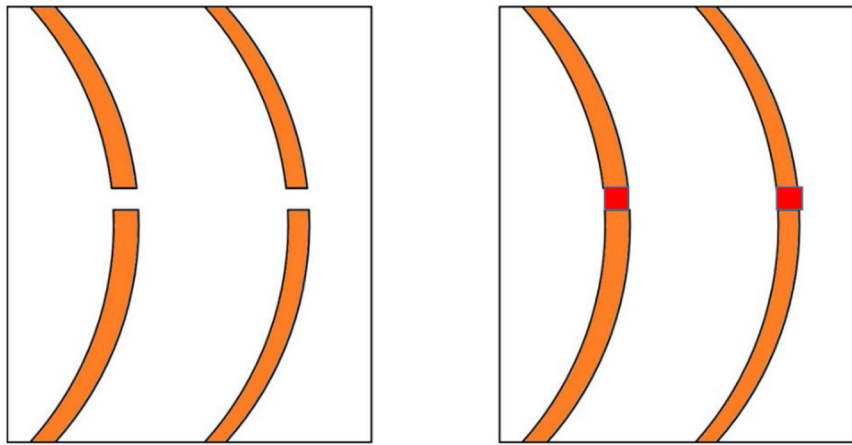


Fig. 9. Simulated surface and its binary form by different thresh-holding methods.



(a) Breakage of continuous tool marks (b) Expected repair of broken tool marks

Fig. 10. Unexpected breakage of tool marks and their repairing scheme.

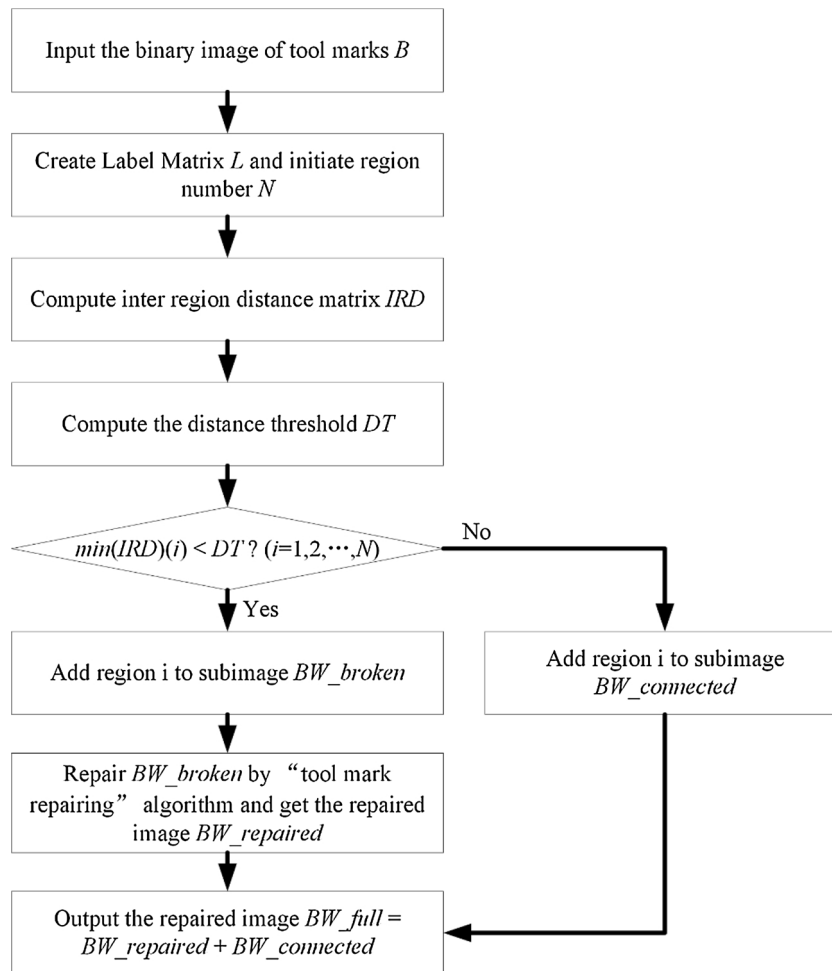
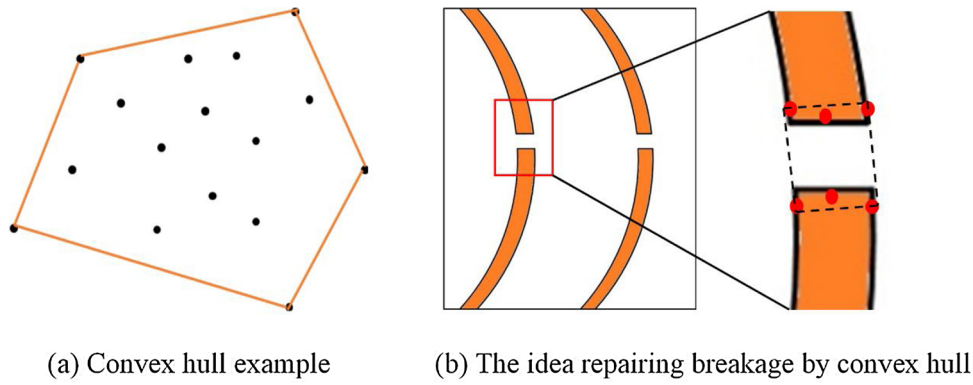


Fig. 11. The work-flow of the broken tool marks identification and repairing.



(a) Convex hull example (b) The idea repairing breakage by convex hull

Fig. 12. The concept of convex hull and its application to repair tool marks' breakage.

Algorithm 1 : Tool mark repairing algorithm

Input: a binary image of broken tool marks BW_broken and distance threshold DT

Output: a binary image of repaired tool marks $BW_repaired$

```

1:   $s = \text{regionprops}(BW\_broken, 'PixelList');$ ;  $len = \text{length}(s)$ ;
     $BW\_repaired = BW\_broken$ ;
2:  For  $i = 1 : len - 1$  do
3:    For  $j = i + 1 : len$  do
4:       $M1 = \text{length}(s(i).PixelList)$ ;  $M2 = \text{length}(s(j).PixelList)$ 
5:      For  $h = 1 : M1$  do
6:        For  $k = 1 : M2$  do
7:          If  $\text{dist}(s(i).PixelList(h, :), s(j).PixelList(k, :)) < 1.5 * DT$  do
8:             $cr = [cr; s(i).PixelList(h, :); s(j).PixelList(k, :)]$ ;
9:          End if
10:         End for
11:        End for
12:        $cr = \text{unique}(cr, 'rows')$ ;  $t = \text{convhull}(cr(:, 1), cr(:, 2))$ ;
13:        $BW\_R = \text{roipoly}(BW\_broken, cr(t, 1), cr(t, 2))$ ;
14:        $BW\_repaired = BW\_repaired + BW\_R$ ;
15:    End for
16:  End for

```

Fig. 13. Tool mark repair algorithm.

line by watershed segmentation is central diagonal except for two ends, as shown in Fig. 15(b).

3. Case study

3.1. Case study I

3.1.1. STRW algorithm experiment

Surfaces produced by milling and turning have apparent periodic tool marks. In this case, the top surface of a B12 cylinder block from an automobile factory is taken as a case to study the proposed surface segmentation methodology. The milling process was carried in an EX-

CELL-O Machining Center using a CBN milling cutter with a diameter of 200 mm. The cutting speed was 1300 rpm, the depth of cut was 0.5 mm, and feed rate was 3360 mm/min. The HDM tool used to measure the cylinder block in this case is ShaPix3D® 3000 series, with a vertical resolution of 0.05 μm and lateral resolution of 150 μm respectively. Its height measurement range is $\pm 5\text{mm}$ and the vertical accuracy is 1 μm . Its field of view is 280 mm \times 280 mm, and the maximum number of sampling points is 4 million in each view. For workpieces whose sizes exceed the field of view, the HDM could stitch multiple point clouds to generate the full view of the surfaces.

A B12 cylinder block is shown in Fig. 16(a) and a sample of its top surface is shown in Fig. 16(b). The partial enlarged view of Fig. 16(b)

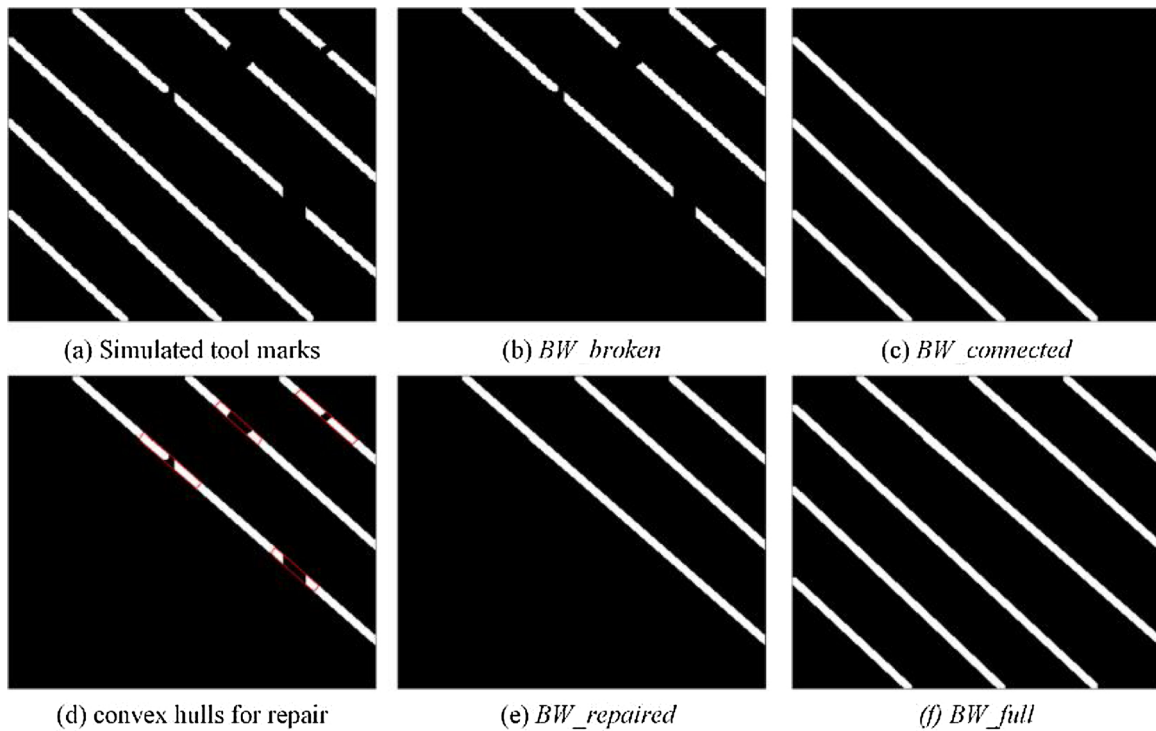


Fig. 14. Simulated tool marks with breakage and its repairing procedures.

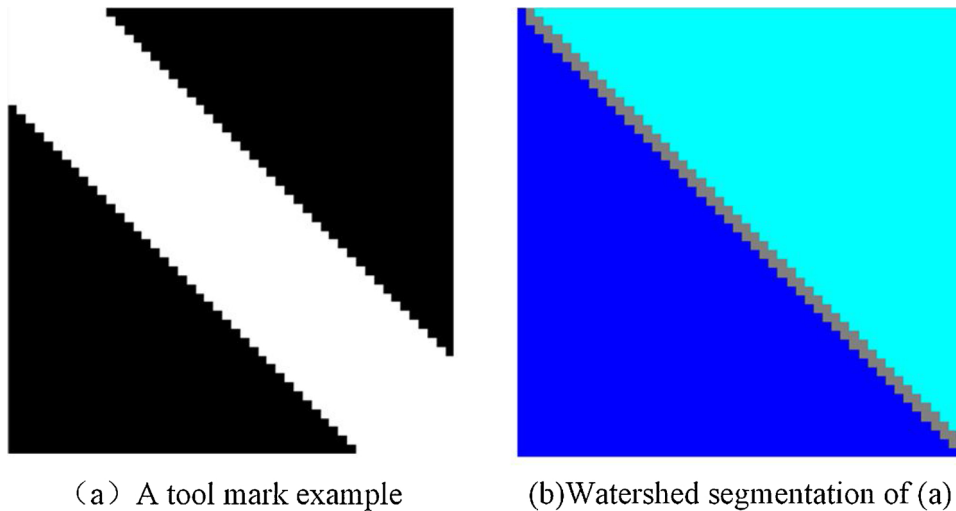


Fig. 15. A diagonal tool mark and its watershed segmentation.

shows obvious periodic tool mark features. For the convenience of showing the segmentation procedures, a small sample of the surface is taken for study, as shown in Fig. 16(b).

A biorthogonal wavelet (bior4.4) is applied to decompose the sampled surface data to different sub-bands, which is shown in Fig. 17.

To select the most suitable subsurface for segmentation, the areal auto-covariance function of each subsurface is calculated and shown in Fig. 18. It is clear that the central point (corresponding to zero offset) is the highest peak in every AACV plot. From the direct vision of Fig. 17, it could be inferred that subsurface D_4 has the strongest periodic degree. The proposed periodic degree values listed in Table 2 also agree with this observation. So the subsurface D_4 is selected for next steps.

The local thresholding result of D_4 is shown in Fig. 19(a). The neighborhood region is defined as a square window of size 7 by 7. And the threshold is $T = 1.4\sigma + m$ (in Eq. (9), a and b are experienced values and may change according to different surface generation methods). In Fig. 19(a), some white blocks appear due to noises. To remove these small noises, the white blocks whose area is less than a certain threshold are discarded. In this case, the threshold value is 10. And the image after noise removal is shown in Fig. 19(b). The labels of each region is shown in Fig. 19(c).

As noticed in Fig. 19(b), there is a breakage occurring in the right-top tool mark. To detect the breakage, the IRD matrix is calculated and listed in Table 3. The last row shows the minimum value of each

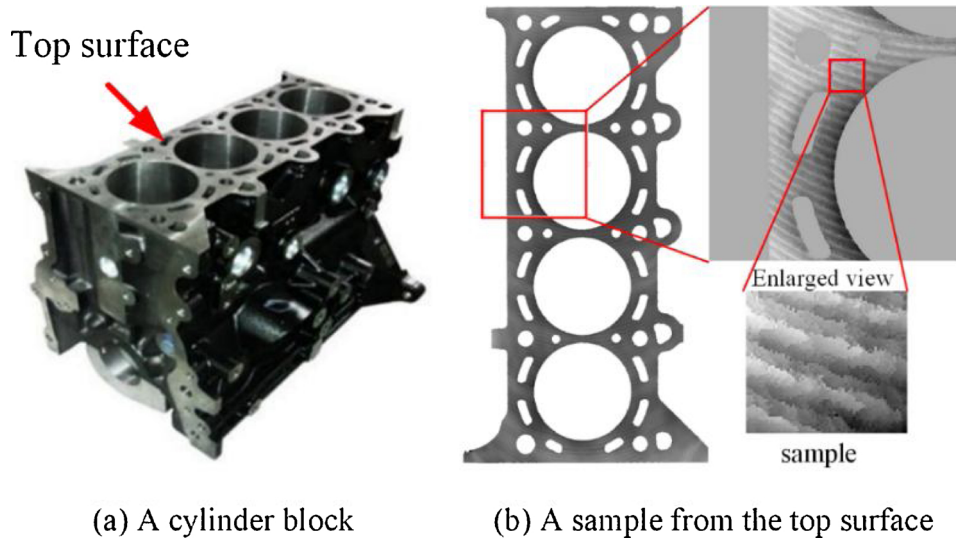


Fig. 16. B12 cylinder block and a sample from its top surface.

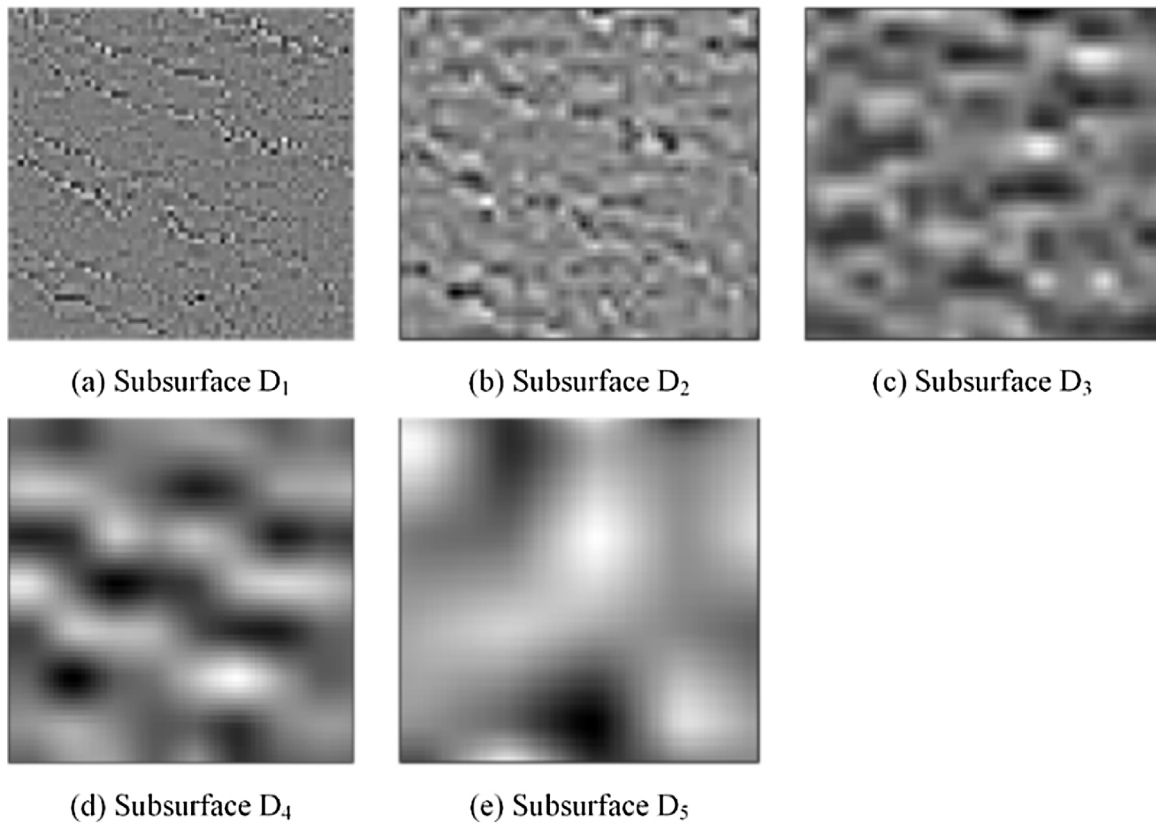


Fig. 17. Decomposed subsurfaces of sampled surface in case1.

column and represents the minimum distance of each region to its nearest neighbor.

Set $C = 0.5$, the distance threshold determined from the last row is $DT = 50 \% \times \max(\min(IRD)) = 50 \% \times 13.34 = 6.67$. According to DT , Region 4 and Region 5 are broken tool marks and need to be re-connected. So Fig. 19(b) can be partitioned into two sub images: one is the broken tool marks BW_{broken} and the other one is connective tool marks $BW_{connected}$. For the broken tool marks shown in Fig. 20(b), “tool mark repair” algorithm proposed in section 2.3 is applied to repair the breakage. The convex hull to repair the breakage is shown by red

boxes in Fig. 20(d). The sub image of repaired tool marks $BW_{repaired}$ is shown in Fig. 20(e). Adding the repaired tool mark image $BW_{repaired}$ with the image of connected tool marks $BW_{connected}$, the fully repaired tool mark image BW_{full} is obtained and shown in Fig. 20(f).

Applying the classical watershed algorithm to the final repaired tool mark image, the segmentation results superimposed on original surface topography and selected subsurface are shown in Fig. 21(a) and (b) respectively. Fig. 21(c) labels each partitioned region with a color for better demonstration. The watershed lines are specially labelled with red color to enhance the vision.

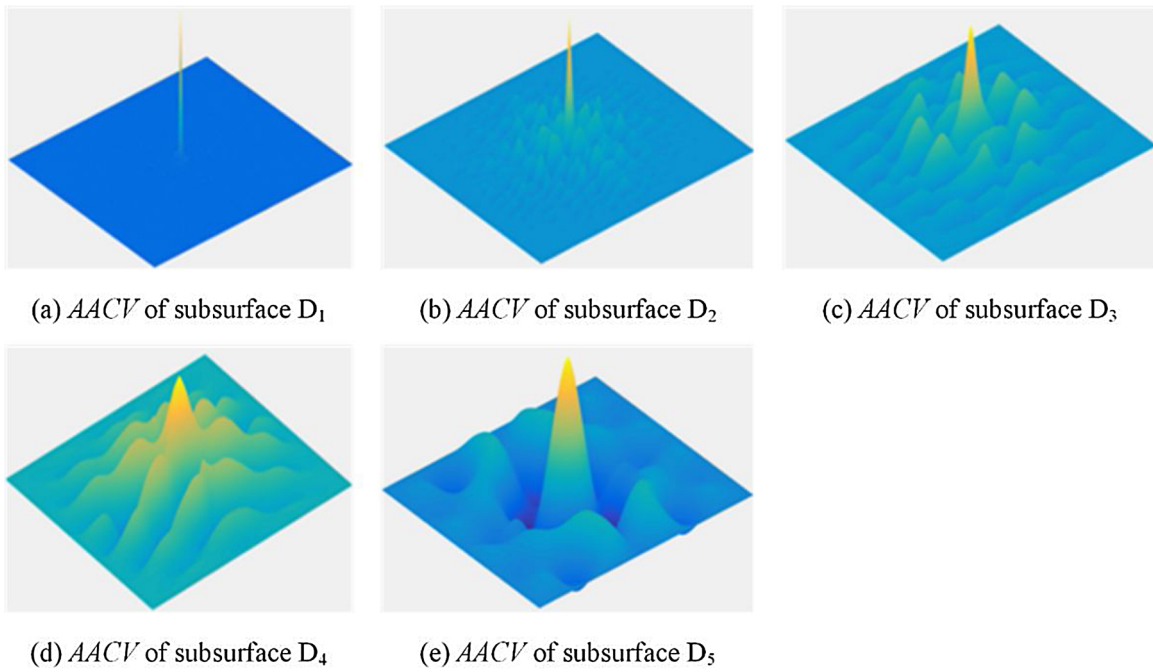


Fig. 18. AACV of subsurface D_1 to D_5 in case1.

Table 2
Periodic degree of subsurface D_1 to D_5 in case1.

Subsurface	D_1	D_2	D_3	D_4	D_5
Periodic degree	0.038	0.181	0.300	0.398	0.045

A cross section perpendicular to tool marks is plotted in Fig. 22. The points on the tool marks are marked with A, B, C and D. It is clear that A, B, C and D are local peak points, which is consistent with the concept of tool marks in Fig. 1. Generally, the tool shape and scar will be negative replicated in surface and repeated at the feed spacing. This phenomenon also holds in this case, the shapes of profile AB, BC and CD are similar to each other. The average feed spacing calculated from Fig. 22(b) is $f = \frac{AB + BC + CD}{3} = \frac{2.7 + 3 + 3}{3} = 2.9mm$. The cutting speed was 1300 rpm, and feed rate was 3360 mm/min. The theoretical feed spacing is $f = \frac{3360}{1300} = 2.58mm$. The relative error is $r = \frac{2.9 - 2.58}{2.58} = 12.4\%$.

Table 3
The inter region distance matrix IRD in case1.

Distance	Region1	Region2	Region3	Region4	Region5
Region1		12.81	31.06	10.77	12.04
Region2	12.81		13.34	30.41	30.41
Region3	31.06	13.34		50.01	51.86
Region4	10.77	30.41	50.01		5.66
Region5	12.04	30.41	51.86	5.66	
$min(IRD)$	10.77	12.81	13.34	5.66	5.66

3.1.2. Comparison with multiscale watershed segmentation algorithm

To compare the segmentation algorithm proposed in this paper with classical methods, the multiscale watershed algorithm proposed by Barré and Lopez [25] is applied to the same surface data. The multiscale watershed algorithm adopts series of area threshold to perform the multiscale watershed segmentation and gains better results in some cases than traditional watershed algorithm. The idea is to fill up non-

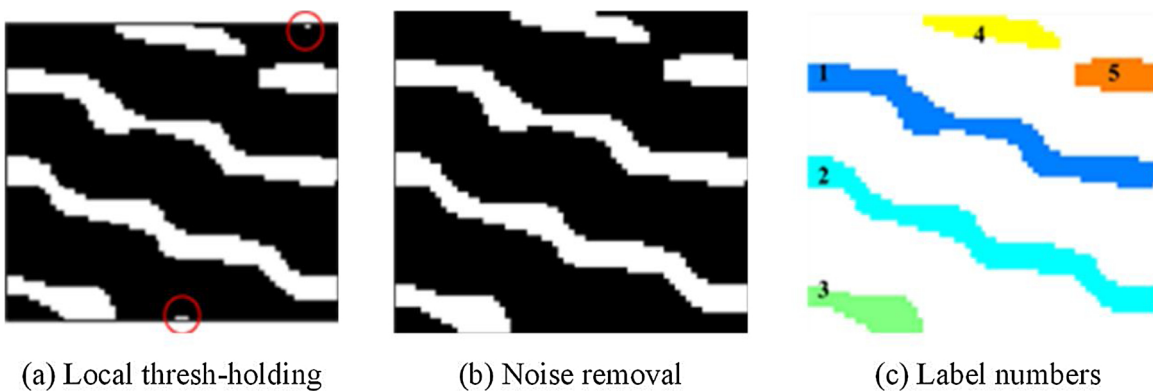


Fig. 19. Local thresholding of D_4 and its noise removal in case1.

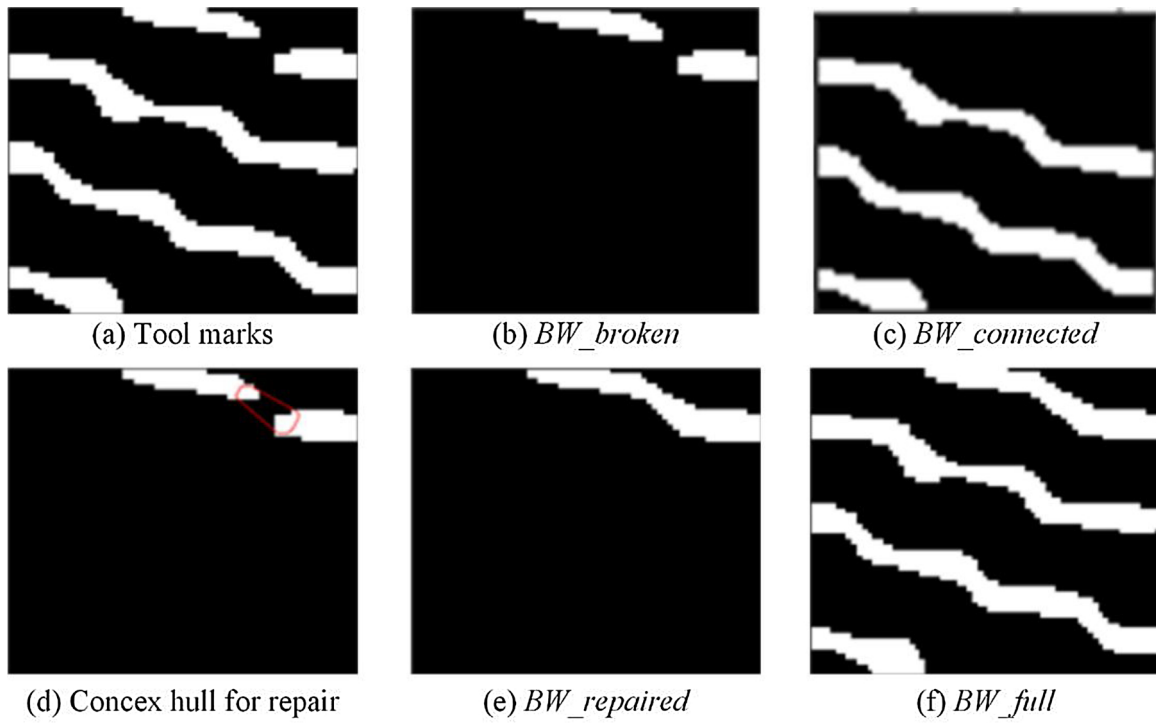


Fig. 20. Tool marks repairing procedures in case1.

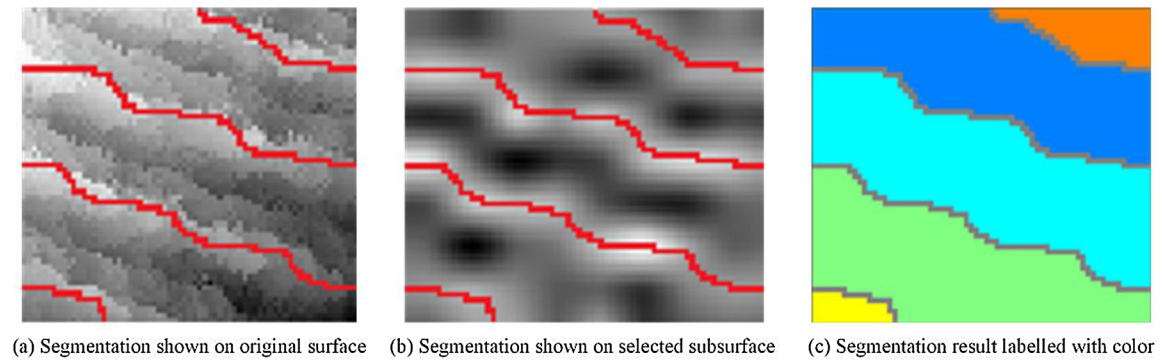


Fig. 21. Final surface segmentation result in case1.

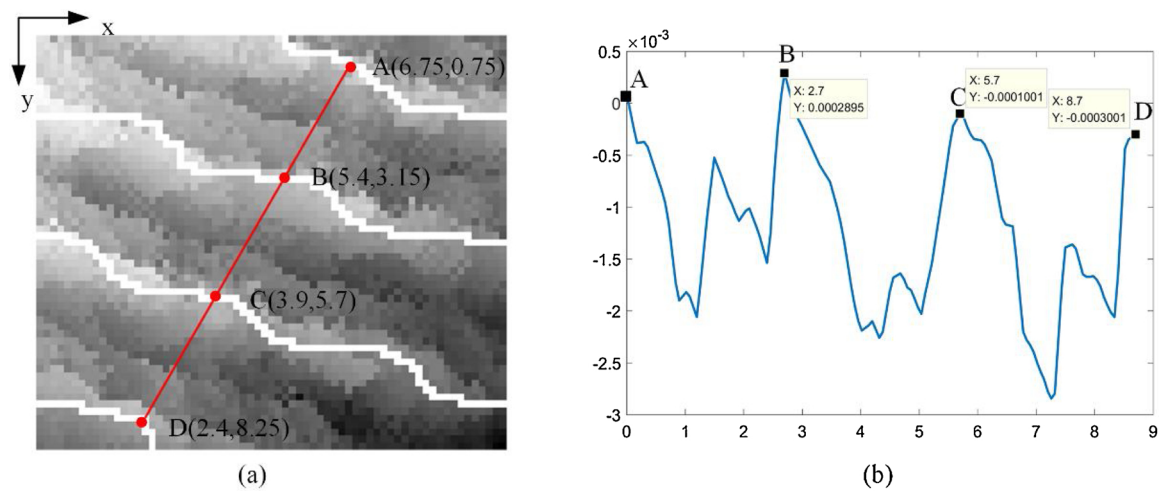


Fig. 22. A cross-section view of tool marks in case1.

Algorithm 2: Multiscale watershed segmentation algorithm

Input: a gray image of surface topography I , area threshold A_{min} , A_{max} and step A_{step}

Output: a cell array of segmentation results S

```

1: For  $A=A_{min}:A_{step}:A_{max}$  do
2:    $L=watershed(I)$ ;  $area = regionprops(L, 'area')$ ;  $min\_area = \min(area)$ ;
3:   While  $min\_area < A$  do
4:      $area\_small = area < A$ ;  $index = \text{find}(area\_small == 1)$ 
5:     For  $i=1:\text{length}(index)$  do
6:        $region = (L == (index(i))); I(region) = \min(I(\text{edge}(region)))$ ;
7:     End for
8:      $L = watershed(I)$ ;  $area = regionprops(L, 'area')$ ;  $min\_area = \min(area)$ ;
9:   End while
10:   $S((A-A_{min})/A_{step}+1) = L$ ;
11: End for

```

Fig. 23. Multiscale watershed segmentation algorithm.

significant catchment basins whose area is less than the threshold and then determine watershed lines for the modified surface to obtain a new segmentation. The pseudocode of this algorithm is shown in Fig. 23.

Fig. 24 shows the multiscale watershed segmentation results and the area threshold A is from 1 to 57.7, equally spaced by interval 8.1. Compared with Fig. 21, it is clear that Fig. 24 has no effective segmentation since the watershed lines are messy and have no physical meanings. And the multiscale segmentation has no trend to approaching the segmented result in Fig. 21 neither. So it could be concluded that traditional watershed segmentation cannot partition the surfaces with periodic tool marks effectively.

Since the B12 engine block top surface is only one of the many types of milled surfaces, other two engineering surfaces are studied in this section to further validate the effectiveness of the proposed methodology.

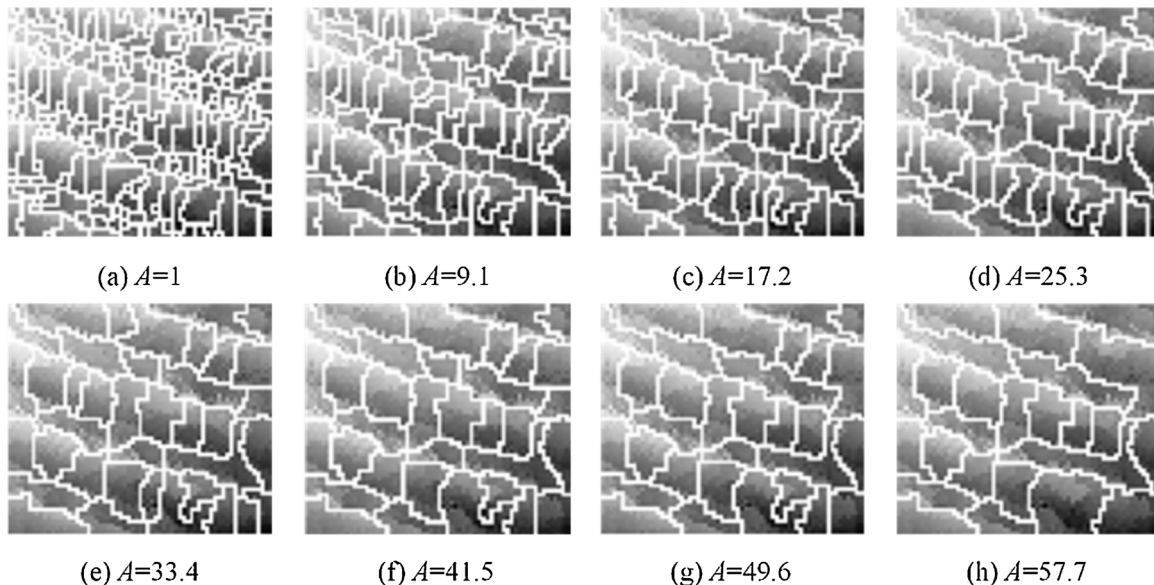


Fig. 24. Results of multiscale watershed segmentation in case1.

3.2. Case study II

A sample from the top surface of a N12 cylinder block is tested in this case. The N12 block was milled with a cutting speed 1200 rpm, a depth of cut 0.6 mm, and a feed rate of 3000 mm/min. Fig. 25 shows a N12 cylinder block and the height map of its top surface measured by Shapix. Similar to case 1, a sample was taken for segmentation. The wavelet (bior4.4) decomposed the sample into subsurfaces (shown in Fig. 26), and their AACV plots are shown in Fig. 27. The periodic degrees of each subsurface are listed in Table 4. Since D_4 has a maximum of periodic degree, D_4 is selected for next steps.

D_4 is locally thresholded by $T = 1.2\sigma + m$ to generate a binary image. Each region of the binary image is labelled and shown in Fig. 28(a). To detect and repair the breakage of tool marks, the IRD matrix is calculated and listed in Table 5. Set $C = 0.8$, the distance threshold determined from the last row is $DT = 0.8 \times \max(\min(IRD)) = 0.8 \times 10.63 = 8.50$. According to DT, Region 1, 3, 4 and 5 are broken tool marks and need to be re-connected. The details of the repairing procedures are shown in Fig. 28.

Applying the classical watershed algorithm to the final repaired tool mark image, the segmentation results are shown in Fig. 29.

A cross section perpendicular to tool marks is plotted in Fig. 30. The points on the tool marks are marked with A, B and C. Although A, B and C are not exactly local peak points, their position are very close to local peaks. The shapes of profile AB and BC are also similar to each other. The average feed spacing calculated from Fig. 30(b) is $f = \frac{AB+BC}{2} = \frac{5.04}{2} = 2.52\text{mm}$. The theoretical feed spacing is $f = \frac{3000}{1200} = 2.5\text{mm}$. The relative error is $r = \frac{2.52-2.5}{2.5} = 0.8\%$.

Fig. 31 shows the multiscale watershed segmentation results and the area threshold A is from 1 to 44.4, equally spaced by interval 6.2. Definitely, the multiscale watershed segmentation cannot partition the surfaces with periodic tool marks into different tool tooth trajectories.

3.3. Case study III

To verify the effectiveness of the proposed algorithm furtherly, a sample from the top surface of a bearing cap is taken for study in this

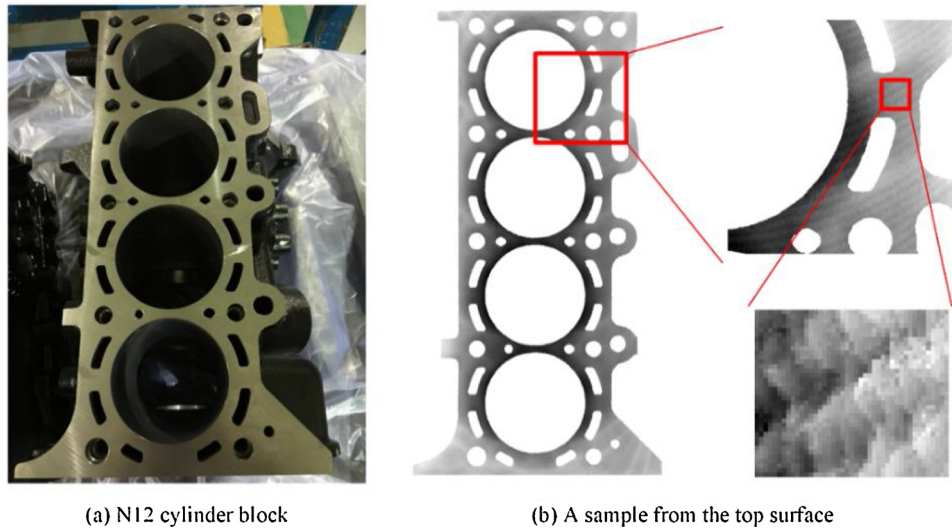


Fig. 25. N12 cylinder block and a sample from its top surface.

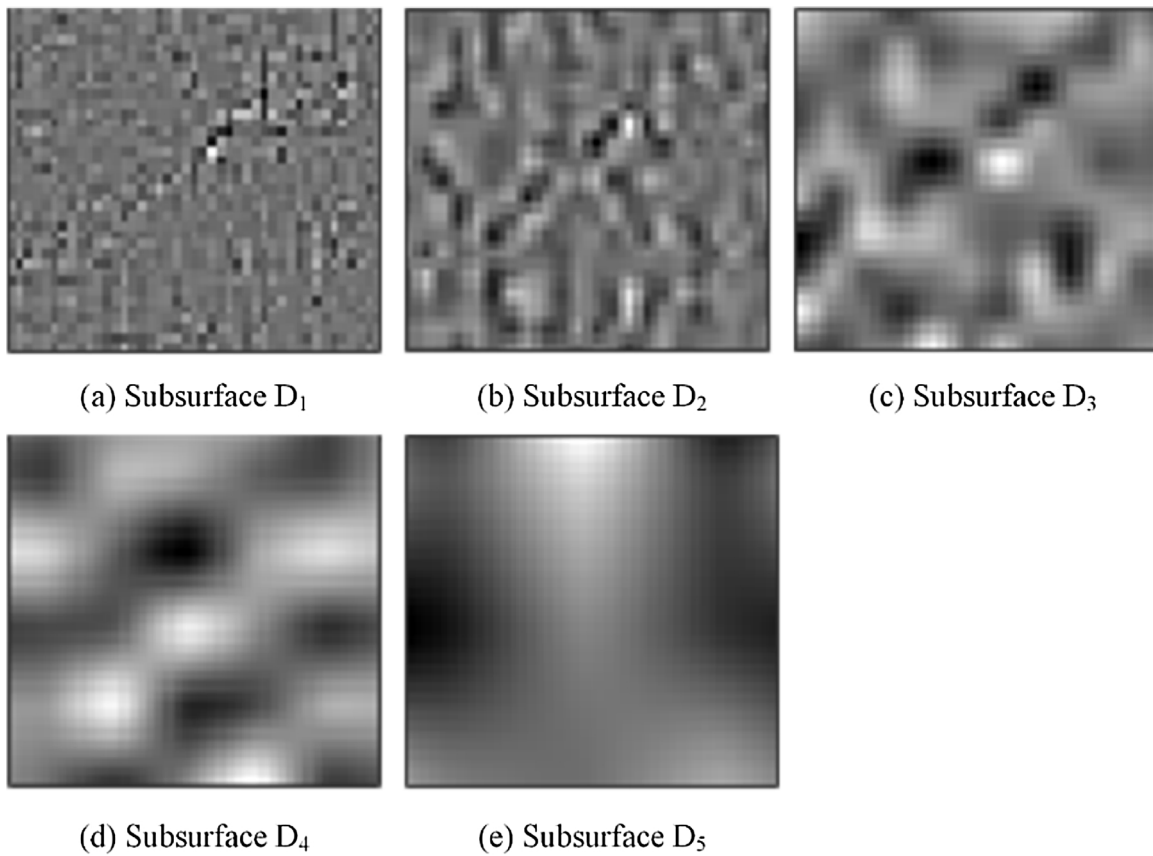


Fig. 26. Decomposed subsurfaces of sampled surface in case2.

case. The top surface of the bearing cap was milled with a cutting speed of 1400 rpm, a depth of cut 0.5 mm and a feed rate of 3800 mm/min. Fig. 32(a) shows a bearing cap. The left top surface was measured by HDM, and the height map is shown in Fig. 32(b). A sample is taken from the measurement to test the proposed methodology.

The wavelet (bior4.4) decomposed subsurfaces and their AACV plots are shown in Fig. 33 and Fig. 34 respectively. The periodic degrees of each subsurface are listed in Table 6. D_4 is selected again, since its periodic degree is maximum.

The local thresh-holding parameters are the same as case 2. The labels of each mark are shown in Fig. 35(a). To detect and repair the

breakage of tool marks, the *IRD* matrix is calculated and listed in Table 7. Set $C = 0.8$, the distance threshold determined from the last row is $DT = 0.8 \times \max(\min(IRD)) = 0.8 \times 10.63 = 8.50$. According to DT , Region 2, 3 and 5 are broken tool marks and need to be re-connected. The details of the repairing procedures are shown in Fig. 35. The final watershed segmentation results are shown in Fig. 36.

A cross section perpendicular to tool marks is plotted in Fig. 37. The points on the tool marks are marked with A, B and C. Although point B is not exactly a local peak, its position is very close to a local peak. The shapes of profile AB and BC are also similar to each other. The average feed spacing calculated from Fig. 37(b) is $f = \frac{AB + BC}{2} = \frac{5.1}{2} = 2.55mm$.

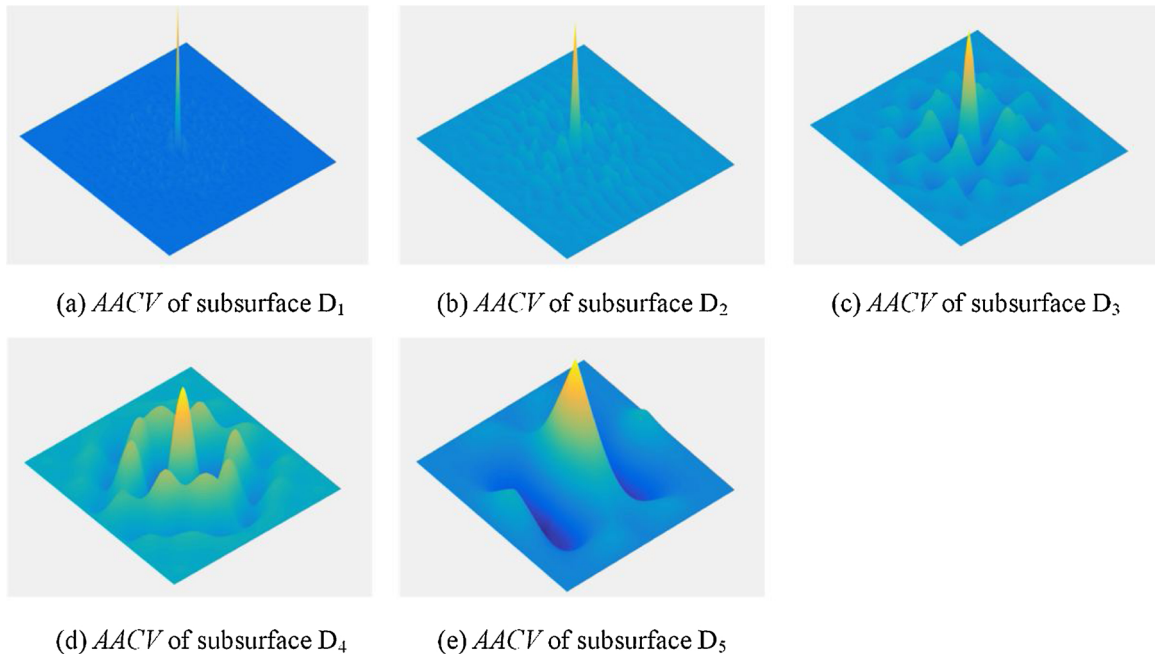


Fig. 27. AACV of subsurface D₁ to D₅ in case2.

Table 4
Periodic degree of subsurface D₁ to D₅ in case2.

Subsurface	D ₁	D ₂	D ₃	D ₄	D ₅
Periodic degree	0.111	0.173	0.273	0.447	0.221

Table 5
The inter region distance matrix IRD in case2.

Distance	Region1	Region2	Region3	Region4	Region5
Region1		12.04	5.66	27.80	31.76
Region2	12.04		10.63	11.40	11.31
Region3	5.66	10.63		29.83	27.46
Region4	27.80	11.40	29.83		7.07
Region5	31.76	11.31	27.46	7.07	
min(IRD)	5.66	10.63	5.66	7.07	7.07

The theoretical feed spacing is $f = \frac{3800}{1400} = 2.71mm$. The relative error is $r = \frac{2.71 - 2.55}{2.71} = 5.9\%$.

Fig. 38 shows the multiscale watershed segmentation results and the

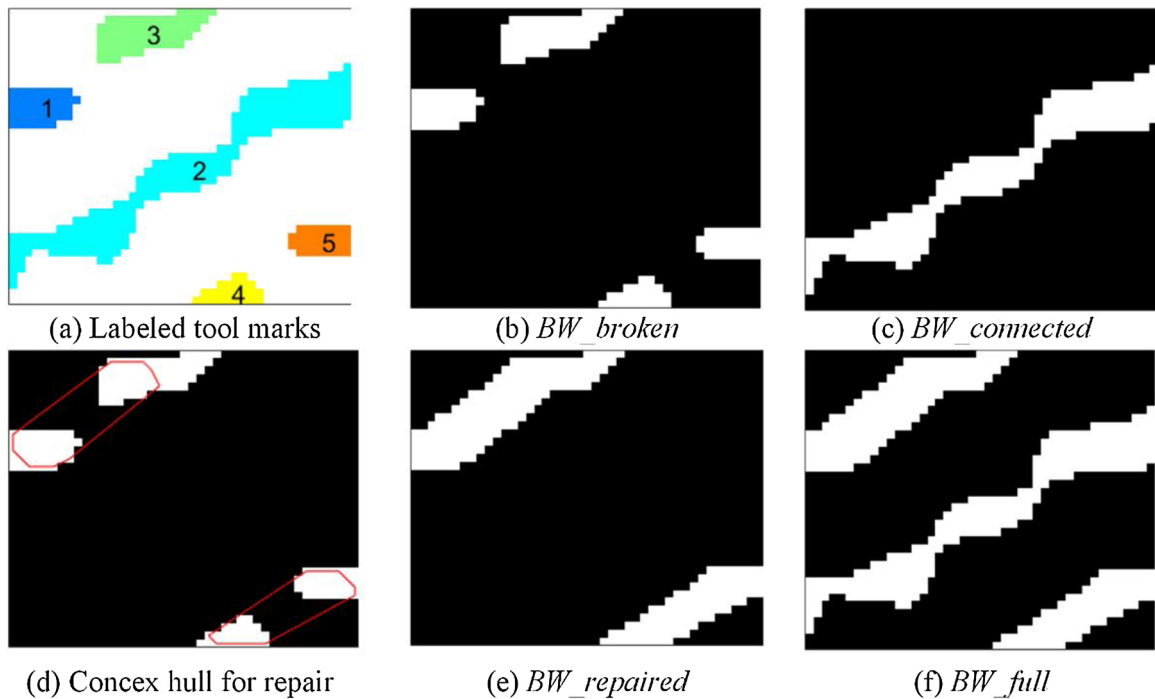
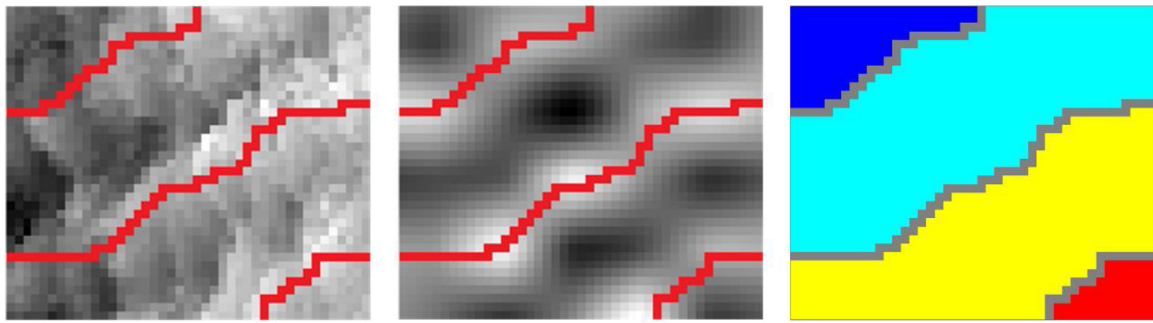


Fig. 28. Tool marks labelling and repairing procedures in case2.



(a) Segmentation shown on original surface (b) Segmentation shown on selected subsurface (c) Segmentation result labelled with color

Fig. 29. Final surface segmentation result in case2.

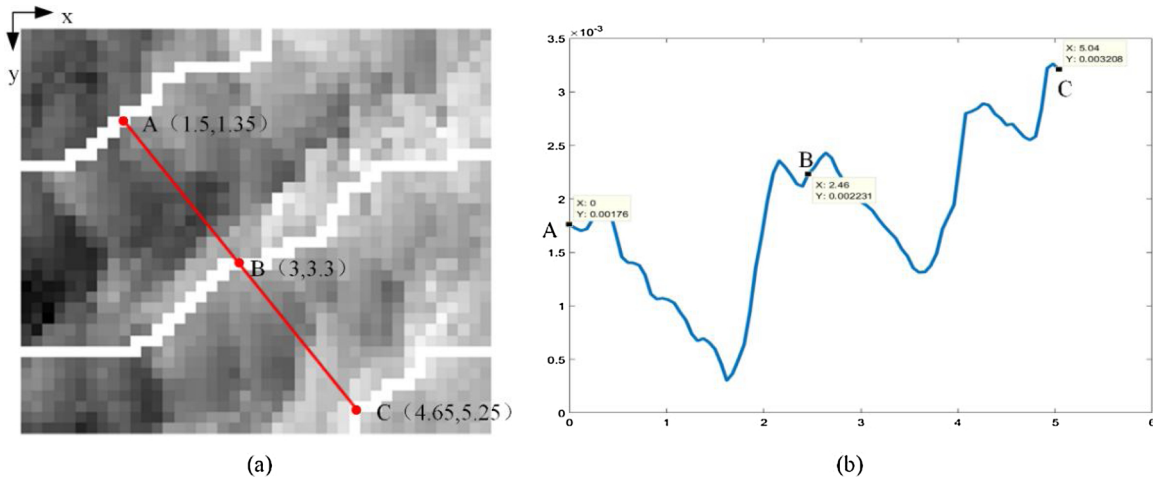


Fig. 30. A cross-section view of tool marks in case2.

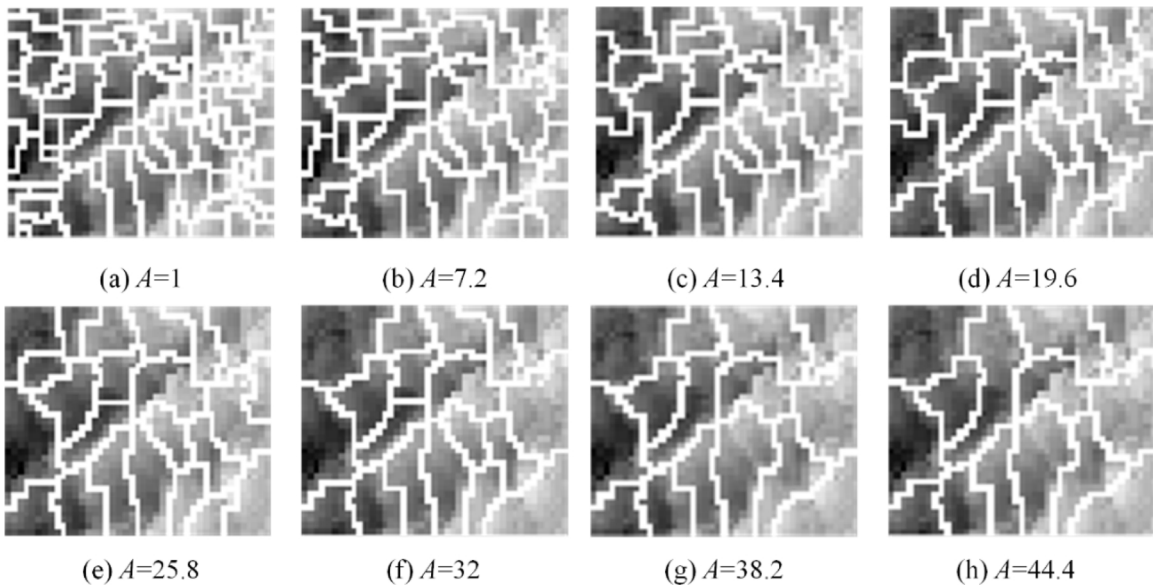


Fig. 31. Results of multiscale watershed segmentation in case2.

area threshold A is from 1 to 50, equally spaced by interval 7. Similar to the conclusion of case 1 and 2, the multiscale watershed segmentation fails to partition the surfaces with periodic tool marks.

In all three cases, the points on tool marks are local peaks or very close to local peaks; each profile segment representing negative replica of tool shape are similar to each other; the calculated feed spacing from

segmentation image is close to the theoretical values calculated from cutting parameters, with an average relative error about 6.4 %. And the multiscale watershed segmentation fails to partition the surfaces correctly in all three cases. Therefore, the conclusion that “STRW” segmentation methodology could effectively divide the milling surfaces with periodic tool marks is drawn.

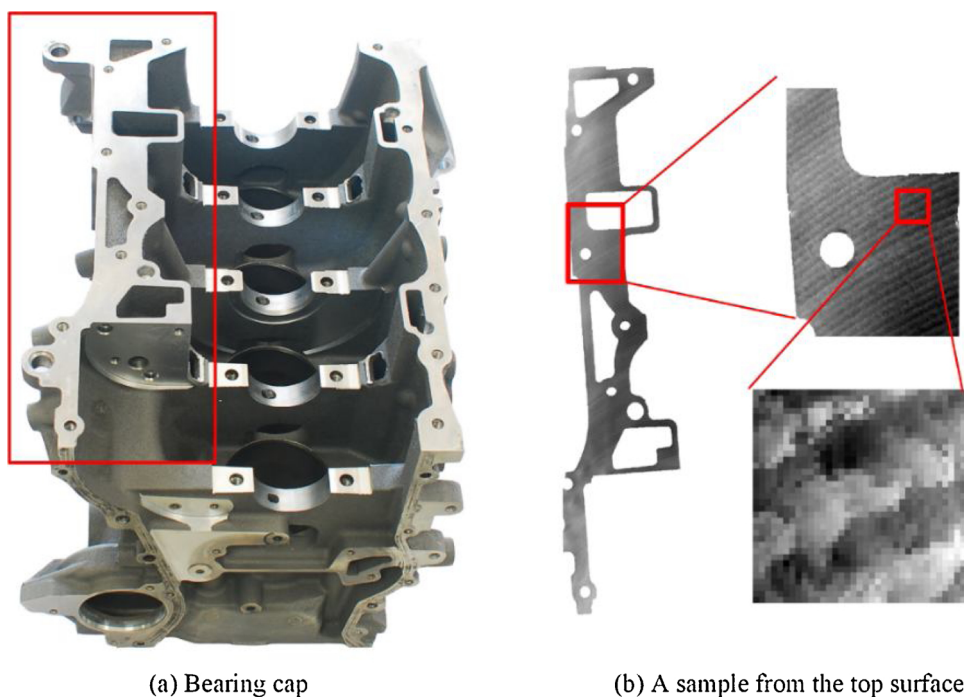


Fig. 32. A bearing cap and a sample from its top surface.

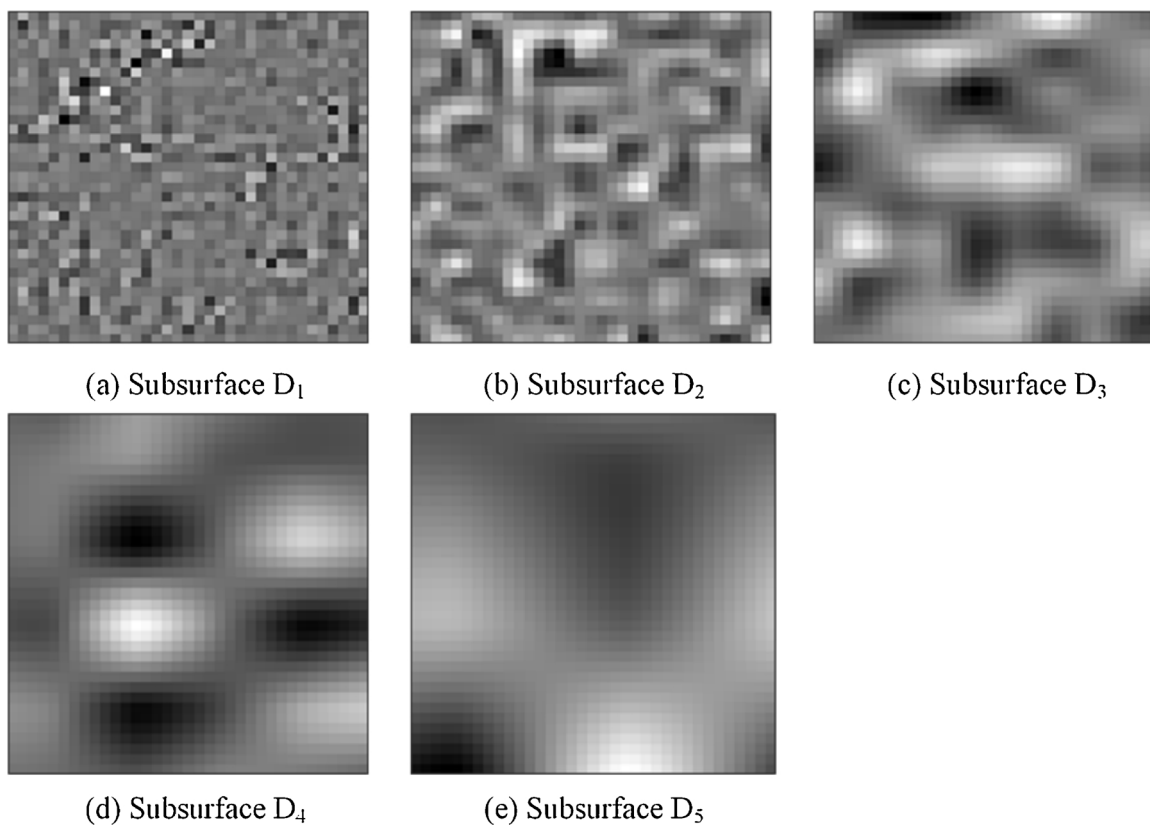


Fig. 33. Decomposed subsurfaces of sampled surface in case3.

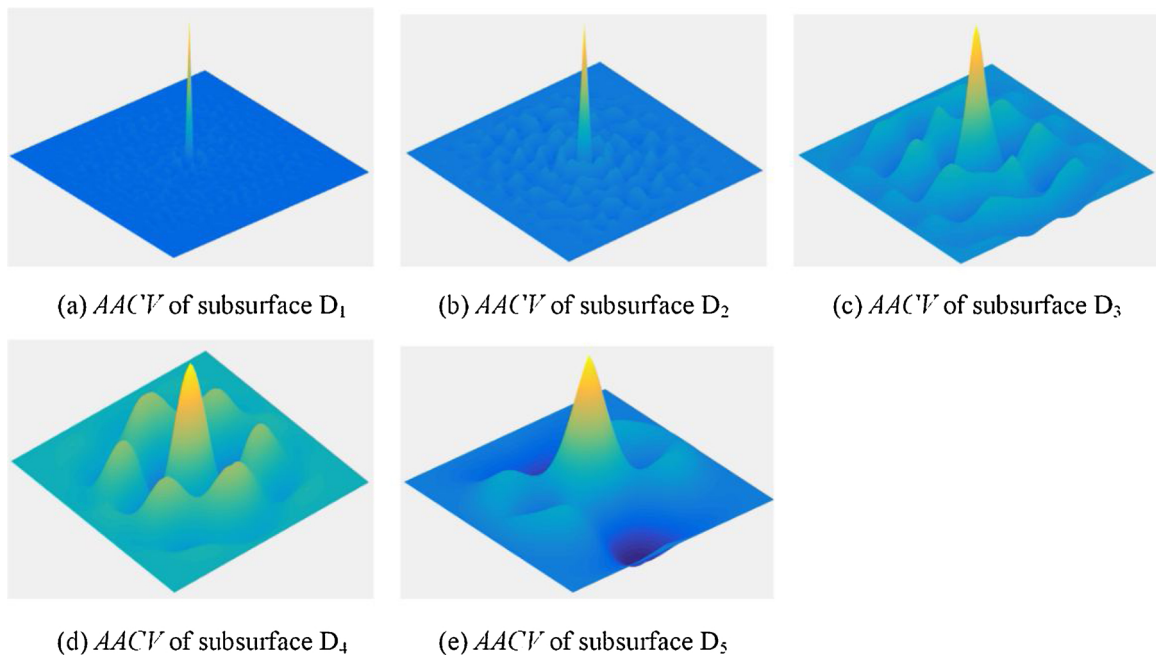


Fig. 34. AACV of subsurface D₁ to D₅ in case3.

Table 6
Periodic degree of subsurface D₁ to D₅ in case3.

Subsurface	D ₁	D ₂	D ₃	D ₄	D ₅
Periodic degree	0.081	0.109	0.237	0.392	0.189

Table 7
The inter region distance matrix IRD in case3.

Distance	Region1	Region2	Region3	Region4	Region5
Region1		15	9.22	27.29	11.31
Region2	15		7.81	18.25	24.41
Region3	9.22	7.81		10.63	7.81
Region4	27.29	18.25	10.63		12.37
Region5	11.31	24.41	7.81	12.37	
min(IRD)	9.22	7.81	7.81	10.63	7.81

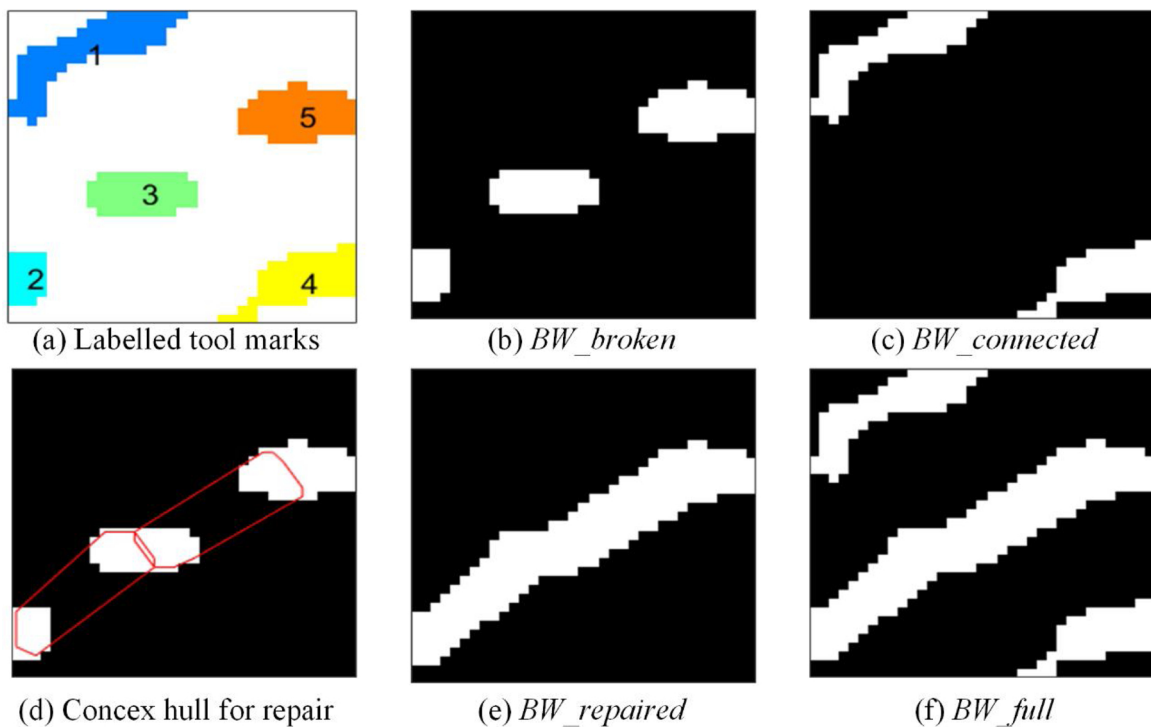
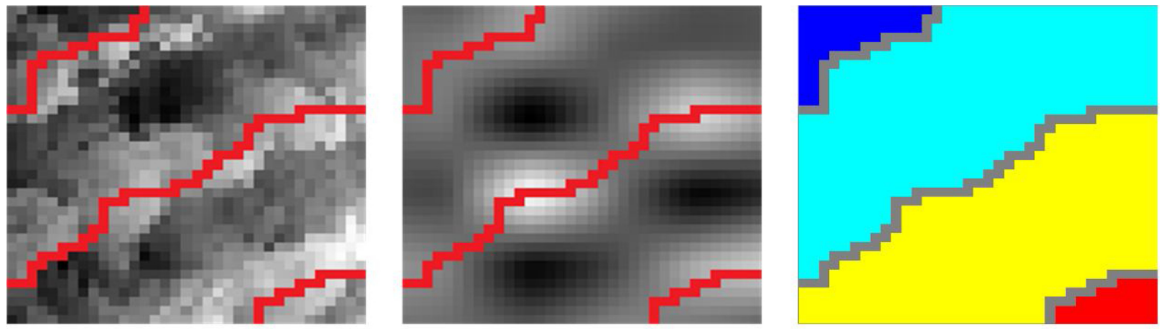


Fig. 35. Tool marks labelling and repairing procedures in case3.



(a) Segmentation shown on original surface (b) Segmentation shown on selected subsurface (c) Segmentation result labelled with color

Fig. 36. Final surface segmentation result in case3.

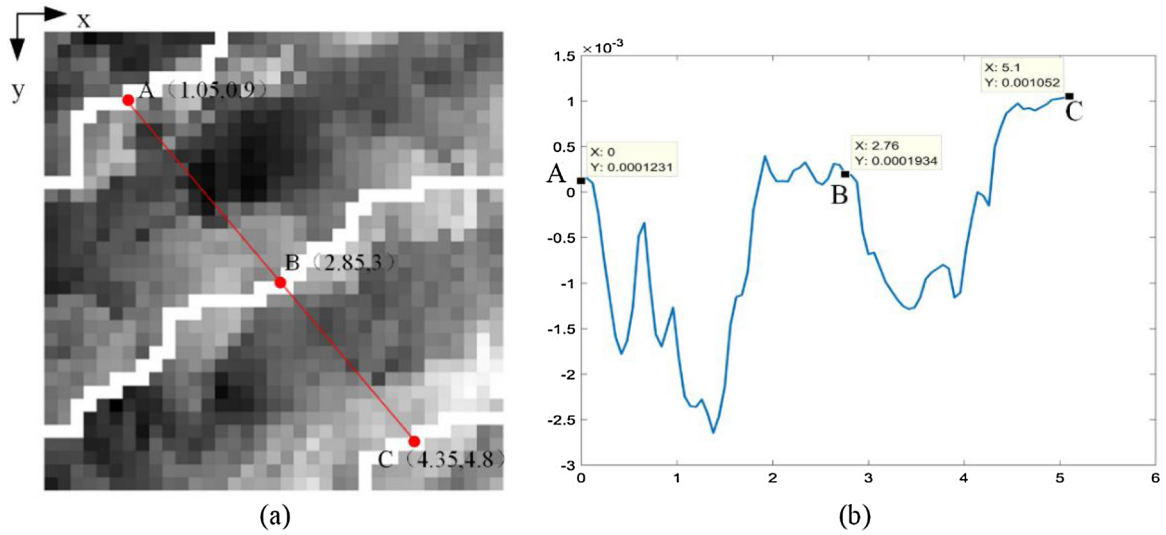


Fig. 37. A cross section view of tool marks in case3.

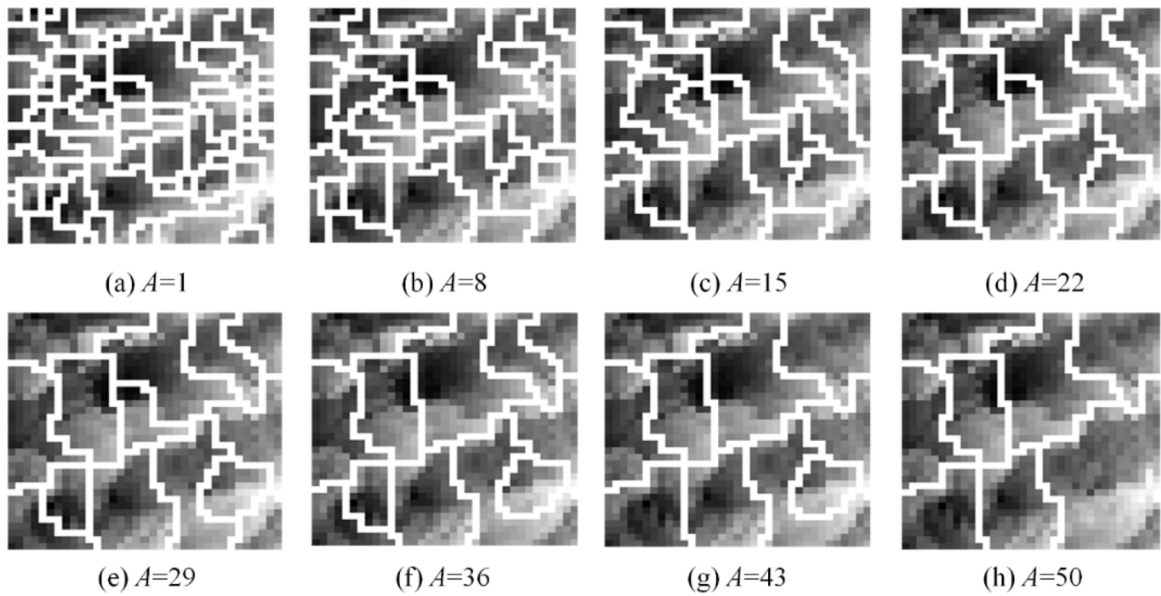


Fig. 38. Results of multiscale watershed segmentation in case3.

4. Conclusion

This paper proposes an improved surface segmentation methodology called “STRW” to partition surfaces with periodic tool marks into distinct regions, and each region belongs to a unique tool tooth trajectory. In the first step, the measured surface is decomposed into different subsurfaces, and a novel concept called “periodic degree” is proposed and used as the criteria of subsurface selection. Then the selected subsurface is locally thresh-held to separate tool marks from its background. Broken tool marks may occur due to surface irregularities, and they are identified by an adaptive distance threshold and repaired by a convex-hull based tool marks repairing algorithm. Finally, the classical watershed segmentation is applied to partition the surface into distinct meaningful regions. The “STRW” segmentation methodology could be an important complement to ISO 16610–85 and it provides a new way to relate surface topography with machining processes.

The proposed “STRW” methodology has well application to continuous surfaces with periodic tool marks. For machined surfaces without periodic tool marks, their segmentation may require special treatment according to their machining processes. For milled surface that has big holes and bores as Fig. 3 shows, additional treatment is required to link the tool marks separated by holes and bores. For the further researches, tool marks on the whole surface of the cylinder block will be classified and parameterized to study the relationship between milling processes parameters and tool marks properties.

Declaration of Competing Interest

The authors declare that they have no known competing financial interests or personal relationships that could have appeared to influence the work reported in this paper.

Acknowledgement

The authors would like to thank Coherix Company for providing the HDM equipment. This work was supported by the National Natural Science Foundation of China (Grant No. 51775343 and No. 51535007).

References

- [1] Marie C, Lasseux D. Experimental leak-rate measurement through a static metal seal. *J Fluids Eng* 2006;129(6):799–805.
- [2] Malburg MC. Surface profile analysis for conformable interfaces. *ASME Trans Manuf Sci Eng* 2003;125(3):624–7.
- [3] Shao YP, Yin YX, Du SC, Xia TB, Xi LF. Leakage monitoring in static sealing interface based on three dimensional surface topography Indicator. *ASME Trans Manuf Sci Eng* 2018;140:101003.
- [4] Liao Y, Stephenson DA, Ni J. Multiple-scale wavelet decomposition, 3D surface feature exaction and applications. *ASME Trans Manuf Sci Eng* 2012;134(1):011005.
- [5] Liu S, Jin S, Zhang XP, Chen K, Tian A, Xi LF. A coupled model for the prediction of surface variation in face milling large-scale workpiece with complex geometry. *ASME Trans Manuf Sci Eng* 2019;141(3):031009.
- [6] Jin S, Liu S, Zhang XP, Chen K. A unified prediction model of 3D surface topography in face milling considering multi-error sources. *Int J Adv Manuf Technol* 2019;102(1):705–17.
- [7] Li PY, Zhai YF, Huang SK, Wang QD, Fu WP, Yang HP. Investigation of the contact performance of machined surface morphology. *Tribol Int* 2017;107:125–34.
- [8] Huang ZH, Shih AJ, Ni J. Laser interferometry hologram registration for three-dimensional precision measurements. *ASME Trans Manuf Sci Eng* 2006;128(4):887–96.
- [9] Wang M, Xi LF, Du SC. 3D surface form error evaluation using high definition metrology. *Precis Eng* 2014;38(1):230–6.
- [10] Shao YP, Yin YX, Du SC, Xi LF. A surface connectivity based approach for leakage channel prediction in static sealing interface. *J Tribol* 2019;141(6):062201.
- [11] Du SC, Liu CP, Huang DL. A shearlet-based separation method of 3D engineering surface using high definition metrology. *Precis Eng* 2015;40:55–73.
- [12] Wang M, Shao YP, Du SC, Xi LF. A diffusion filter for discontinuous surface measured by high definition metrology. *Int J Precis Eng Manuf* 2015;16(10):2057–62.
- [13] Shao YP, Wang K, Du SC, Xi LF. High definition metrology enabled three dimensional discontinuous surface filtering by extended tetrolet transform. *J Manuf Syst* 2018;49:75–92.
- [14] Du SC, Liu T, Huang DL, Li GL. A fast and adaptive bi-dimensional empirical mode decomposition approach for filtering of workpiece surfaces using high definition metrology. *J Manuf Syst* 2018;46:247–63.
- [15] Du SC, Huang DL, Wang H. An adaptive support vector machine-based workpiece surface classification system using high-definition metrology. *IEEE Trans Instrum Meas* 2015;64(10):2590–604.
- [16] Du SC, Liu CP, Xi LF. A selective multiclass support vector machine ensemble classifier for engineering surface classification using high definition metrology. *ASME Trans Manuf Sci Eng* 2015;137(1):011003.
- [17] Wang M, Du SC, Xi LF. Predicting machined surface topography based on high definition metrology. 15th IFAC Symposium on Information Control Problems in Manufacturing INCOM 2015:1013–7.
- [18] Shao YP, Du SC, Xi LF. 3D machined surface topography forecasting with space-time multioutput support vector regression using High definition metrology. 37th Computers and Information in Engineering Conference Cleveland, Ohio, USA 2017:V001T002A069.
- [19] Shichang Du LX. High definition metrology based surface quality control and applications. Singapore: Springer; 2019.
- [20] Nguyen HT, Wang H, Hu SJ. Characterization of cutting force induced surface shape variation in face milling using high-definition metrology. *ASME Trans Manuf Sci Eng* 2013;135(4):041014.
- [21] Nguyen HT, Wang H, Hu SJ. Modeling cutter tilt and cutter-spindle stiffness for machine condition monitoring in face milling using high-definition surface metrology. *Int J Adv Manuf Technol* 2014;70(5–8):1323–35.
- [22] Wang M, Ken T, Du SC, Xi LF. Tool wear monitoring of wiper inserts in multi-insert face milling using three-dimensional surface form indicators. *ASME Trans Manuf Sci Eng* 2015;137(3):031006.
- [23] ISO. Geometrical product specifications(GPS)-filtration Part 85: morphological areal filter: segmentation. Geneva,Switzerland: International Organization for Standardization; 2013. Standard No. ISO 16610-85:2013.
- [24] Bleau A, Leon LJ. Watershed-based segmentation and region merging. *Comput Vis Image Underst* 2000;77(3):317–70.
- [25] Barré F, Lopez J. Watershed lines and catchment basins: a new 3D-motif method. *Int J Mach Tools Manuf* 2000;40(8):1171–84.
- [26] ISO. Geometrical product specifications (GPS)-Surface texture: Areal-Part2: terms, definitions and texture parameters. Geneva,Switzerland: International Organization for Standardization; 2012. Standard No. ISO 25178-2:2012.
- [27] Otsu N. A threshold selection method from gray-level histograms. *IEEE Trans Syst Man Cybern* 1979;9(1):62–6.
- [28] Barber CB, Dobkin DP, Huhdanpaa H. The quickhull algorithm for convex hulls. *ACM Trans Math Softw* 1996;22(4):469–83.